Cement and Concrete Composites 125 (2022) 104319

Contents lists available at ScienceDirect

Cement and Concrete Composites

journal homepage: www.elsevier.com/locate/cemconcomp

Low-temperature (−10 °C) curing of Portland cement paste – Synergetic effects of chloride-free antifreeze admixture, C–S–H seeds, and room-temperature pre-curing

Ahmad Alzaza [a], Katja Ohenoja [a], Isak Langås [b], Bård Arntsen [b], Minna Poikelispää [c], Mirja Illikainen [a,*]

[a] Fibre and Particle Engineering Research Unit, Faculty of Technology, University of Oulu, P.O. Box 4300, 90014, Oulu, Finland
[b] Department for Infrastructure, Materials, and Construction. Sintef Narvik AS, Postboks 250, 8504, Narvik, Norway
[c] Tampere University, Faculty of Engineering and Natural Sciences, P.O. Box 589, FI-33014, Tampere, Finland

ARTICLE INFO

Keywords:
Cold weather
Curing temperature
Nucleation
Seeding
CO_2 emissions
Water absorption

ABSTRACT

Cold weather drastically shortens the construction season in northern regions. Low ambient temperatures are known to have detrimental impacts on the reactivity and hardened performance of cementitious materials. This study therefore aims to assess the combined impacts of calcium silicate hydrate (C–S–H) seeds, binary chloride-free antifreeze admixture (i.e., urea and calcium nitrate), and short-period precuring at room temperature (23 ± 1 °C) on ordinary Portland cement (OPC) paste-cured at −10 °C. The heat of hydration, setting time, compressive strength, freezing point, frozen water amount, hydration products precipitation rate, water absorption, and permeable porosity were investigated experimentally. The best results in terms of compressive strength, degree of hydration, water absorption, and permeable porosity were obtained when C–S–H seeds, antifreeze admixture, and precuring were combined due to their mutual impacts. In the absence of room-temperature precuring, C–S–H seeds additive and antifreeze admixture showed negligible acceleration impacts on compressive strength development of subzero-cured paste. The incorporation of seeds and antifreeze admixture decreased the freezing points of the binders and thus protected the admixed binders against frost damage, and their effects were more obvious when combined with a few hours of precuring. The compressive strength of 28 d-old OPC paste modified by C–S–H seeds and antifreeze admixture and treated with precuring developed rapidly at −10 °C, gaining 96% (75.1 MPa) of that measured in control paste cured at room temperature (78 MPa), with comparable durability properties and a significant reduction of energy consumption and CO_2 emissions.

1. Introduction

Urbanization and infrastructure development are constantly increasing worldwide. In northern regions, the harsh cold weather significantly shortens construction and maintenance seasons because of its detrimental impacts on cementitious materials' quality. This slows down infrastructure developments and construction schedules in those areas. The American concrete institute (ACI) defines weather as "cold weather" when the air temperature is below 4 °C for more than three consecutive days and not higher than 10 °C for 12 h [1]. These weather conditions are common in northern regions for at least 4–6 months yearly.

Curing temperature is known to be a critical factor affecting the hydration rate of ordinary Portland cement (OPC). Several studies have reported an accelerated hydration rate for cementitious materials with increasing curing temperature [2,3], whereas low curing temperatures are known for their deacceleration impacts on hydration rate due to the diminished dissolution rate of cement particles and the increased apparent activation energy (E_a) of the chemical reaction of the hydration process [4–7]. The apparent E_a of cement hydration is defined as the potential energy barrier between reactant and reaction product precipitation [5]. Therefore, low curing temperatures prolong the setting time and deaccelerate the early strength development of cementitious materials. Furthermore, subzero curing temperatures can damage the microstructures of cementitious systems via frost damage resulting from the 9% volume expansion of ice [8,9]. Microstructural damages due to

* Corresponding author.
E-mail address: Mirja.Illikainen@oulu.fi (M. Illikainen).

https://doi.org/10.1016/j.cemconcomp.2021.104319
Received 14 June 2021; Received in revised form 8 September 2021; Accepted 18 October 2021
Available online 22 October 2021

early freezing can halve the final strength and frost resistance of ordinary Portland cement (OPC) concrete, even though the strength gain is re-established when the concrete is thawed during warm months [10,11]. Consequently, several measures, including antifreeze admixtures, thermal systems, heated raw materials, and special cement types (e.g., rapid-hardening cement and calcium sulphoaluminate cement) have been employed in winter construction activities, especially when the ambient temperature is < 5 °C [1,10,12–17]. These measures aim to protect the fresh concrete against freezing during its plastic and hardening states, as well as accelerating the early hydration reaction of the cement. Among these strategies, the usage of antifreeze admixtures in cold weather concreting works is the most economical and easily applicable option [9,15].

Antifreeze admixtures are a cost-efficient way of depressing the freezing point of mixing water [9,10,15,16,18–21]. Calcium-containing antifreeze admixtures, such as calcium nitrate ($Ca(NO_3)_2$) and calcium chloride ($CaCl_2$), contain the same Ca^{2+} as alite (C_3S) and belite (C_2S), the main mineral phases of OPC, and thereby, hydration processes intensify in their presence, which shortens the setting time and accelerates the strength development rate, even at a low temperature [17]. Therefore, $CaCl_2$ and $Ca(NO_3)_2$ are considered multifunctional admixtures for cementitious material. Despite the good performance of $CaCl_2$ as an antifreeze/acceleration admixture, the presence of chloride increases the corrosion risk of reinforcing bars embedded in concrete. This has renewed interest in developing chloride-free antifreeze admixtures and accelerators. Several researchers [9,10,15,21] assessed the efficiency of various chloride-free antifreeze admixtures in OPC-based systems. They reported that mutual impacts on the part of binary antifreeze admixtures (e.g., urea/calcium nitrate and sodium thiocyanate/calcium nitrate) on cement hydration and strength development under subzero curing temperatures are more significant than those detected with the use of only antifreeze admixture. Karagol [10] showed that the compressive strength of 28 d-old admixed OPC-based concrete prepared with binary antifreeze admixture (i.e., urea/calcium nitrate) and cured at −10 °C was 25 times higher (25 MPa) than that of the control sample (1.3 MPa). Similar observations were also reported by Khan and Kumar [9], who used sodium thiocyanate/calcium nitrate as a binary antifreeze admixture in OPC concrete. However, despite the depressed freezing point of admixed samples with an antifreeze admixture, the strength development rate at subzero curing temperatures is significantly slower than that at standard curing due to decreased cement dissolution, reactivity, and hydration product precipitation rates [22]. This extends construction schedules and increases the costs of construction works.

The incorporation of nanosized particles (NPs) in cementitious materials is attracting increasing interest. Due to their high surface area, NPs exhibit high surface reactivity and the ability to provide additional foreign nucleation sites for hydration product precipitation, thus accelerating cement hydration [23,24]. Therefore, the inclusion of NPs enables the development of cementitious materials with superior hardened and durability properties for special uses. Several NPs were investigated and used in cement research, such as nano-SiO_2, nano--Al_2O_3, nano-Fe_2O_3, nano-TiO_2, nano-$CaCO_3$, and nano-clays [5,25–32]. Recently, calcium silicate hydrate (C–S–H) seeds revealed the best acceleration performance in cementitious materials with no side impact on late-age strength as compared to other NPs and accelerators [33–35]. Also, C–S–H seeds have been successfully employed as nucleation agents to accelerate the hydration of cement, leading to a shorter induction period and higher cumulative heat flow, as monitored by isothermal calorimetry [35–37]. More recently, Zhang et al. [38] assessed the impacts of C–S–H seeds on OPC-based paste cured at −5 °C and showed that the strength development of OPC-based binders was enhanced with the inclusion of C–S–H seeds. They attributed the strength development enhancement to the nucleation impacts of the seeds. In addition, Zhang et al. [38] reported that the incorporation of C–S–H seeds enhanced the dissolution of OPC, thereby depressing the freezing point of the pore solution because of its increased ion concentration. According to their findings, −6 °C was the lowest measured freezing point, and this value was observed in the binder containing 5% C–S–H seeds. However, in northern regions, ambient temperatures usually drop below −6 °C during the winter season, which will result in the freezing of the binder, thus stopping reaction progress and strength development.

Therefore, this work aims to assess the synergic impacts of C–S–H seeds and antifreeze admixtures on OPC binder cured at −10 °C. In addition, the effects of short-period precuring at room temperature (23 ± 1 °C) on reactivity and strength development of subzero temperature-cured OPC-based paste were thoroughly investigated. The influences of C–S–H seed content, with and without antifreeze admixture, on the heat of hydration during the precuring period, were investigated via isothermal calorimetry. The freezing point and the amount of frozen water were measured using low-temperature differential scanning calorimetry (LT-DSC). X-ray diffraction (XRD) and thermogravimetric analysis (TGA) were used to evaluate the hydration progress and precipitation rates of hydrates. The microstructural assessment was performed using scanning electron microscopy (SEM). In addition, the hardness and durability properties of the pastes were assessed in terms of compressive strength, water absorption, and permeable porosity, and setting time was also measured.

2. Materials and experimental methods

Ordinary Portland cement (CEM I 52.5 R) provided by Finnsementti, Finland, was used. The density, Blaine fineness, and median particle size (D_{50}) of cement are around 3100 kg/m^3, 400 m^2/kg, and 8.5 μm, respectively. The chemical composition of OPC is given in Table 1. A commercial C–S–H seed admixture (X130-seeds®) was supplied by MBCC, Sweden, with a solid content of around 23.7% (measured after drying at 105 °C until a constant mass was achieved). The foil-like amorphous morphology of the C–S–H seeds was captured via transmission electron microscopy (TEM, JEM-2200FS, Japan) and shown in Fig. 1. A detailed seed characterization can be found in the producer-registered patent [39]. A polycarboxylate-based superplasticizer with no retarding effects, which is named Viscocrete-5800 (provided by Sika®, Finland and complied with EN 934-2 requirements for water-reducing additives and superplasticizer) and has a solid content of approximately 35.5%, was used. Chloride-free antifreeze admixtures, namely urea (NH_2CONH_2) and calcium nitrate ($Ca(NO_3)_2{\cdot}4H_2O$), were employed in this study. The chemical compositions of urea and calcium nitrate are listed in Table 2. Deionized water was used. All materials were stored under lab-controlled conditions at 23 ± 1 °C and 60% relative humidity, with no special heating treatment before mixing.

2.1. Paste preparation and curing conditions

Ten binders were developed in this work to investigate the impacts of C–S–H seeds, antifreeze admixtures, and 6 h-precuring (23 ± 1 °C) on the strength development of OPC-based binders cured at −10 °C. Table 3 lists the proportions of the mix compositions. First, the SP (0.5 wt% of cement) and C–S–H seed solution (0, 0.5, 2, 4, 6 wt% of cement) were added to the mixing water and maintained in an ultrasonic bath (Elmasonic P, Germany) for 5 min [25]. For binders with the binary antifreeze admixture, solid urea and calcium nitrate (at a mass ratio of 1:1 and a total of 6 wt% of cement) were first dissolved in the mixing water 24 h before mixing and kept capped at room temperature (23 ± 1 °C). The early preparation of antifreeze admixture was due to the endothermic dissolution reaction of urea in water, which leads to a

Table 1
Chemical composition of CEM I 52.5R.

Elemental oxides	CaO	SiO_2	Al_2O_3	Fe_2O_3	MgO	SO_3	LOI
Composition (% wt.)	69.0	24.0	2.1	0.3	0.7	2.3	0.8

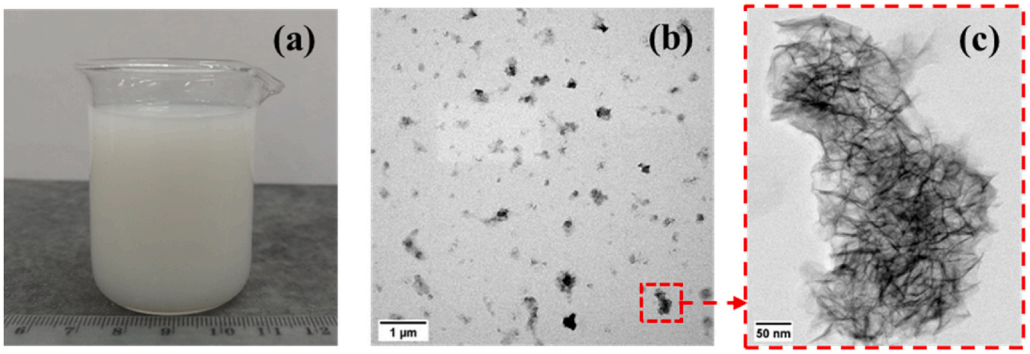

Fig. 1. (a) As-received C–S–H seeds solution (X130®, MBCC), (b) TEM imaging of C–S–H seeds (agglomeration due to drying procedure during sample preparation), and (c) zoomed TEM image.

Table 2
Chemical properties of calcium nitrate ($Ca(NO_3)_2{\cdot}4H_2O$, 99% pure) and urea (NH_2CONH_2, 99–100% pure).

Chemical composition	Calcium nitrate	Urea
Cl	≤0.005%	≤5 ppm
SO_4	≤0.002%	≤0.001%
NO_2	≤0.005%	***
Fe	≤5 ppm	≤0.001%
Heavy metals	≤5 ppm	≤0.001%
pH	5–7	***
Solubility in water	1470 g/L	480 g/L

Table 3
Mix proportions of the study.

Sample ID	PC (g)	C–S–H seeds solution (g)	SP(1)(g)	AF(2) (g)	w/c(3)	Mixing solution/c volume ratio[a]
C0	100	0	0.5	0	0.27	0.84
C0.5		0.5				
C2		2				
C4		4				
C6		6				
C0AF		0		6 (3g of calcium nitrate + 3g of urea)	0.23	
C0.5AF		0.5				
C2AF		2				
C4AF		4				
C6AF		6				

(1): superplasticizer, (2): binary antifreeze admixture, (3): water-to-cement mass ratio.
[a] Considering dissolved binary antifreeze admixture (when used) and water content in C–S–H seed solution and SP solutions.

significant decrease in mixing solution temperature [40–42]. Then, SP and seed solution were added to the antifreeze admixture-containing solution, following the procedures mentioned above. For mix compositions without the binary antifreeze admixture, the water-to-cement mass ratio (w/c) was kept constant at 0.27 (considering the amount of water in the SP and C–S–H seed solution). Dissolving the binary antifreeze admixture in the mixing water increases the total volume of the mixing solution (binary antifreeze admixture + water) and changes the solution-to-cement volume ratio, which is known to impact the consistency, early hydration reaction, and hardened properties of cementitious materials [42]. Therefore, in this work, the w/c ratio of mix compositions prepared with antifreeze was adjusted to 0.23 (considering the amount of water in the SP and C–S–H seed solution), so that the mixing water/solution-to-cement volume ratio was maintained at 0.84 for all mixes. The OPC and mixing water/solution were mixed for 3 min and then cast in 20 × 20 × 20 mm^3 molds, vibrated, and sealed with a plastic sheet to avoid early moisture loss [11]. Thereafter, the pastes in the molds were cured in a pre-set freezer (−10 ± 0.5 °C) for up to 28 d. To study the impact of the precuring period on the properties of OPC-based pastes cured at subzero temperatures, similar binders were cast and allowed to cure at room temperature for 6 h while sealed; then, the samples were placed in the freezer (−10 ± 0.5 °C) for up to 28 d.

To mimic the conditions at construction sites, molds for freezer-cured samples without the 6 h of precuring were maintained in the freezer (−10 °C) for one day before casting, whereas the molds for the samples with the 6 h of precuring were maintained at room temperature.

For the sample coding, C0-(0 h) refers to the control paste cured at −10 °C without precuring, whereas C6-(6 h) indicates the samples prepared with 6% C–S–H seeds and precured for 6 h at room temperature before being cured at subzero temperatures. C6AF-(6 h) refers the 6 h-precured samples prepared with 6% C–S–H seeds and the binary antifreeze admixture.

2.2. Testing methods

2.2.1. Heat of hydration

The heat release evolution was monitored using an isothermal calorimeter (Thermometrics TAM air) to monitor the impacts of C–S–H seed content and binary antifreeze admixture on the reaction rate during the precuring period (i.e., 6 h at room temperature). The calorimeter's internal temperature was set at 23 °C and equilibrated for 1 d. Samples were prepared according to Section 2.1. Thereafter, around 3–5g of the pastes were poured into glass ampules. Water was used as a reference sample. The results were normalized using the mass of the pastes.

2.2.2. Setting time

An automated Vicat apparatus (Matest E044 N, Italy) was used to measure the setting time of paste samples at 23 ± 1 °C according to the EN196-3 standard [43]. The initial and final setting times were reported at needle penetrations of 6 ± 3 mm and 39.5 mm to the bottom, respectively, while using a mold 40 mm in height.

2.2.3. Low-temperature differential scanning calorimetry (LT-DSC)

To assess the influences of C–S–H seeds, antifreeze admixture, and precuring on the freezing point of and amount of frozen water (i.e., free water) in the pastes, low-temperature differential scanning calorimetry (LT-DSC, Netzsch Polyma 214, Germany) was used. Samples were prepared according to Section 2.1, and around 50–60 mg was poured into aluminum crucibles. Thereafter, the pastes in the crucibles were subjected to rapid cooling, followed by rapid heating conditions. For pastes with no 6 h-precuring, crucibles containing freshly mixed binders were placed immediately in the machine, and the test was performed with the following temperature program: at −30 °C for 5 min, then raised from −30 °C to 25 °C at a rate of 5 °C/min [12]. For pastes with the precuring, the crucibles were sealed and stored at room temperature for 6hr and

then tested following the above procedures.

Thereafter, the freezing points and amount of frozen water were determined using the LT-DSC heat flow curve of the phase-change materials (Fig. 2). In the cementitious materials, the phase change of the hydration products does not take place within the temperature range of −30 °C – 25 °C, and the only phase change that occurs is related to the pore solution [8]. The melting of the frozen water results in an endothermic peak. The temperature at the intersection of the tangent line and baseline of the initial melting curve is considered to be the melting point of frozen water (i.e., the freezing point) (Fig. 2a) [8,12]. Furthermore, the integral area of the melting peak can be considered to be the amount of frozen water in the frozen paste samples [44].

2.2.4. Hydration evolution and products

A Precisa prepASH 129 (Precisa Gravimetrics AG, Dietikon, Switzerland) was used to collect the TGA data. At the designated time, the hydration was stopped via the solvent exchange technique using isopropanol, and the solution was changed twice during the first 2 h at 1-h intervals and then kept in fresh isopropanol for 48 h [11]. Then, the samples were dried in a desiccator at room temperature until the analysis date. Samples were crushed and powdered, and the specimens were then heated from 25 °C to 1000 °C at 10 °C/min in an inert nitrogen atmosphere. Chemically bound water (CBW) was then calculated and corrected for the loss of ignition (LOI) at 950 °C and calcite content in anhydrous OPC (Equation [1]) [45].

$$CBW = Ldh + Ldx + 0.41(Ldc - Ldc_a) - \quad m_c(LOI) \tag{1}$$

$$m_c = \frac{m_s}{(1 + w/c) \times (1 + LOI)} \tag{2}$$

where Ldh, Ldx, and Ldc are the mass losses due to the dehydration and decomposition of ettringite (80–400 °C and 600–750 °C [46]), dihydroxylation (400–580 °C), and decarbonation (750–1000 °C), respectively [47],

Ldc_a is the mass loss due to the decomposition of calcite ($CaCO_3$) from an anhydrous sample, 0.41 is the conversion factor used to calculate the amount of bound water from the decomposition of $CaCO_3$, m_c is the mass of cement contained in the sample and can be calculated using Equation (2), and m_s is the sample mass.

The XRD analysis of the samples was performed using a Rigaku SmartLab diffractometer (Tokyo, Japan) under the following conditions: a voltage of 40 kV, current of 135 mA, step size of 0.02°, scanning speed of 4°2Θ/min, and scanning range of 2Θ = 5°–130°. Phase identification was performed using X'pert HighScore Plus (PANalytical software).

2.2.5. Compressive strength

The compression test was carried out using 20 mm cubic paste samples prepared according to Section 2.1. A calibrated Zwick/Roell (Z400) compressive test machine with a load cell of 100 kN was used. The average and standard deviation for six cubes were reported for each data point. It should be stated that the unadmixed samples (without antifreeze admixture) were stored for around 60 min at room temperature before testing to eliminate the potential impacts of any formed ice in the pore structure [11,48].

2.2.6. Scanning electron microscopy

The microstructures of selected pastes were investigated using field emission scanning electron microscopy (Zeiss ULTRA plus FESEM, Germany). The analysis was carried out using carbon-coated specimens under a backscatter electron detector at an acceleration voltage of 15 kV. The hydration stoppage of the samples used was performed as mentioned above in Section 2.2.4.

2.2.7. Water absorption and permeable porosity

Typically, the water absorption of OPC-based binders is measured according to ASTM C642 [49] recommendations, where samples are dried at 105 °C until the mass difference between the two consecutive measurements is ≤ 0.5%. However, recently, Thériné et al. [50] proved that the oven-drying method at a high temperature (i.e., 105 °C) can decompose some hydrates (e.g. ettringite), double the pore size, and increase the porosity of the OPC-based paste. The latter resulted in a 40% increase in water absorption when compared to similar pastes dried at 20–30 °C. Similarly, Tian et al. [51] dried cement mortars at 60 °C, instead of 105 °C for similar above-mentioned reasons.

Therefore, the vacuum-oven drying method at 30 °C was adopted in this study. However, the drying period at low temperature can be long, which will permit the subzero-cured samples to react, densifying the microstructure with newly precipitated hydration products due to the increased curing temperature, as reported earlier [11,38]. To tackle this challenge, the intact 28 d-old subzero-cured samples (six cubes/mix) were entirely immersed in isopropanol (at a solvent/paste volume ratio of 10:1 [52]), and the solution was changed every 1 h during the first 2 h and, then, every 2 days to guarantee complete water removal [2]. The soaking time in isopropanol ends when the difference between two consecutive surface-dry isopropanol-saturated masses was less than 0.5%, and this process requires 7–14 days, depending on sample permeability. It is worth mentioning that the containers containing samples immersed in isopropanol were kept in the freezer (−10 °C) to limit the impact of increased surrounding temperature on the reactivity of the pastes.

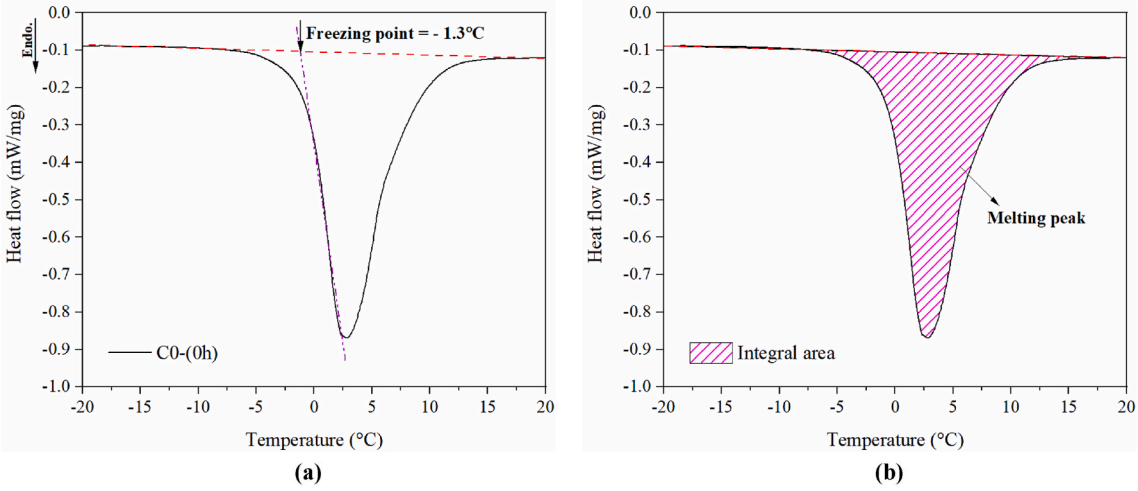

Fig. 2. LT-DSC heat flow curve of C0 (with 0 h precuring): (a) determination of freezing point; and (b) melting heat (i.e., the amount of frozen water).

Thereafter, samples were dried in an oven vacuum at 30 °C, and oven-dry mass (M_D) was reported when the difference between the two measurements was ≤0.5%. The dried samples were then fully immersed in a water container (23 ± 1 °C) for 48 h. After the immersion period, the buoyant mass (M_B) of cubes and surface dry water-saturated mass (M_{sat}) were registered. Water absorption and permeable porosity were calculated using Equation (3) and Equation (4), respectively.

For comparison purposes, a second portion of the samples was dried at 105 °C, without the isopropanol immersion step, and water absorption and permeable porosity were measured following the above-mentioned procedures.

$$\text{Water absorption } (\%) = \left(\frac{M_{sat} - M_D}{M_D}\right) \times 100 \quad (3)$$

$$\text{Permeable porosity } (\%) = \left(\frac{M_{sat} - M_D}{M_{sat} - M_B}\right) \times 100 \quad (4)$$

3. Results and discussion

3.1. Paste behavior during the precuring period

3.1.1. Heat of hydration

The inclusion of C–S–H seeds and/or antifreeze admixture accelerated the hydration rate of the binders according to the hydration heat measurement (see Fig. 3). The acceleration impact was more significant at higher C–S–H seed dosages and with the mutual addition of seeds and antifreeze admixture. The heat flow and cumulative released heat were measured to explore the hydration progress of the binders during the 6 h precuring period at room temperature.

The values of the main acceleration peaks and the reductions in the time needed to reach the peaks (T_P) were increased with increased C–S–H seed content (see Fig. 3a). Therefore, T_p (and acceleration peak value) were 9 h (6.6 mW/g), 8.6 h (7.3 mW/g), 7.1 h (7.4 mW/g), 6.4 h (8 mW/g), and 6 h (8.2 mW/g) in C0, C0.5, C2, C4, and C6, respectively. This shows that the maximum reduction (≈33.3%) in the induction phase period was gained by the addition of 6 wt% of C–S–H seeds, while the minimum (≈4.4%) was calculated at low seed dosages (i.e., 0.5 wt%) in comparison with C0. Moreover, the cumulative heat released during the precuring period (H_{6h}) at room temperature was consistent with the heat flow trend, as shown in Fig. 3b. Thus, H_{6h} was significantly increased with the addition of C–S–H seeds, and the increase was more obvious in the binders synthesized with seed content ≥2 wt%. Therefore, H_{6h} values of around 4.7, 4.9, 8.7, 14.7, and 17.2 J/g were measured in C0, C0.5, C2, C4, and C6, respectively.

With the addition of antifreeze admixture, the hydration rates of the binders were further accelerated and enhanced, regardless of the presence of C–S–H seeds (Fig. 3a). Therefore, the acceleration peak of C0AF appeared 2.2 h (24.4%) earlier than C0. Similarly, the H_{6h} value of C0AF (14.6 J/g) was 5 times higher than that measured in C0 (4.7 J/g). Due to the mutual effects of the binary antifreeze admixture and C–S–H seeds, T_p and H_{6h} were further shortened and enhanced, respectively, when compared to the impacts of seeds or antifreeze admixture alone. Thus, the main hydration peaks were reached 2.2, 3.3, 4.3, and 4.5 h earlier in C0.5AF, C2AF, C4AF, and C6AF, respectively, than the control binder (i.e., C0). Similarly, the values of H_{6h} were considerably increased, and values around 15.1, 19.5, 24.6, and 27 J/g were measured in C0.5AF, C2AF, C4AF, and C6AF, respectively, as compared to C0. The higher heat released at an early age (6 h at room temperature) with seed inclusion and the addition of the binary antifreeze admixture indicates a more drastic hydration process and reaction product precipitation during the precuring period.

The accelerated hydration in the seeded binders can be credited to the nucleation effects of the added C–S–H seeds in the binders, which accelerate the kinetics of the cement hydration process, with a prominent effect on the induction and acceleration periods. The reported acceleration impacts of the embedded C–S–H seeds are consistent with the literature [35,38,46]. Shortly after mixing a cement paste, the nuclei of the C–S–H gel begin to precipitate over the anhydrous cement particles [5]. In the presence of added C–S–H seeds, additional nucleation sites are available in the pore solution, favoring the precipitation of the hydration products over these sites and away from cement particles [5,35,37,38]. This modified precipitation mechanism will hinder or at least lessen the formation of a thick semi-impermeable hydration product barrier around anhydrous cement particles [53]. This barrier is known to limit the diffusivity of water toward anhydrous cement particles, as well as the release of the ions from cement particles to the pore solution, thereby negatively affecting the follow-up hydration [54,55]. Moreover, enhancing the hydration products' precipitation rate in the presence of additional nucleation sites can accelerate the consumption rate of ions from the pore solution, which creates a concentration gradient away from the cement particles and improves the subsequent cement particles' dissolution and hydration rates [56].

Furthermore, the accelerated T_p with the addition of the binary antifreeze admixture is mainly due to the presence of $Ca(NO_3)_2$. Justnes and Nygaard [57] proved the acceleration impact of $Ca(NO_3)_2$ on the early hydration process of OPC-based binder at room temperature, especially at an early age. Similarly, Didamony et al. [58], Kičaitė et al. [59], Choi et al. [60], and Li et al. [61] reported that $Ca(NO_3)_2$ accelerated the solubility and hydration of the alite (C_3S), belite (C_2S), and tri-calcium aluminate (C_3A) phases in OPC. The enhancements were

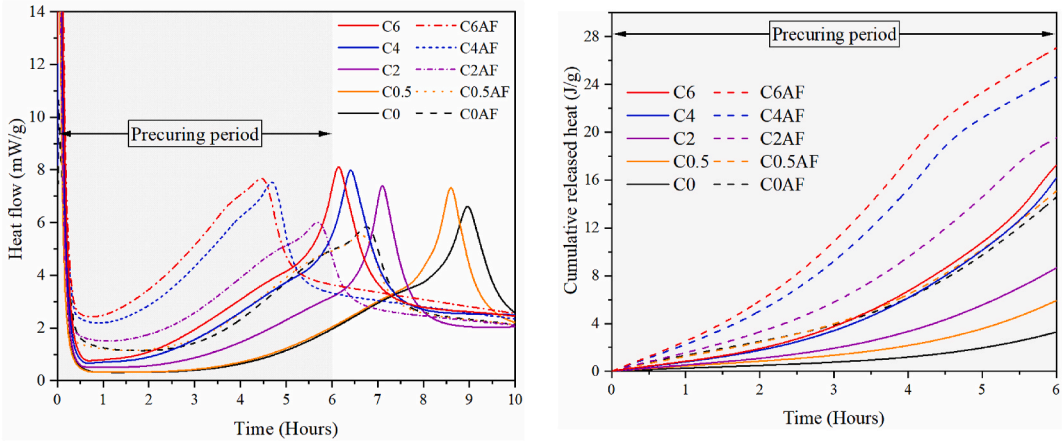

(a) (b)

Fig. 3. (a) Heat flow evolution and (b) cumulative heat of hydration of pastes at 23 °C.

mainly attributed to the increased concentration of Ca^{2+} in the pore solution with the presence of $Ca(NO_3)_2$, which accelerated the formation of cement hydration product (i.e., C–S–H) [59]. In addition, with the presence of $Ca(NO_3)_2$, the nitrate ions (NO_3^-) react rapidly with Al_2O_3 in the C_3A phase, generating additional nitrate hydrates [NO_3-ettringite (AFt) and NO_3-monosulfate (AFm)], in addition to the SO_4^{2-}-AFt that is typically formed through the hydration of OPC [60,62]. The formation of the nitrate hydrates was proven via XRD and TGA/DTG (as shown below in Section 3.3.1). The precipitation of these additional nitrate-based hydration products indicates the accelerated T_p in the antifreeze admixture-containing pastes. The findings of this work are in line with the literature [57,59,63,64]. On the other hand, despite the higher heat flow rate noted during the first 6 h (i.e., the precuring period) in C0AF, C0.5AF, and C2AF as compared to C0, C0.5, and C2, respectively, a decrease in the peak values of the former was found. The latter is in line with the findings of Kicaite et al. [17] and Wang et al. [45], who reported a decrease in hydration acceleration peak value in OPC-based materials with the addition of 3 wt% $Ca(NO_3)_2$ and ≥5 wt% urea, respectively. Promisingly, high C–S–H seed content (≥4 wt%) in C4AF and C6AF compensated for the peak reduction caused by the addition of the binary antifreeze admixture. Moreover, Wang et al. [45] stated that the addition of urea can retard the reactivity of the OPC/fly ash binder and postpone the occurrence of its main hydration peak. According to the results of this study, it is obvious that the presence of C–S–H seeds and $Ca(NO_3)_2$ can completely compensate for the retardation impact (if any) of urea antifreeze admixture, and thus, no retarding behavior was detected. It is worth noting that $Ca(NO_3)_2$ and urea were chosen due to their high efficiency in depressing the freezing point of the mixing solution, cost-effectiveness, and high solubility [10,17].

3.1.2. Setting time

The initial and final setting times of the pastes were significantly shortened with C–S–H seed content and binary antifreeze admixture addition (Fig. 4). This is in line with the shortened induction period and accelerated appearance of the acceleration peaks, as observed previously in Fig. 3a. According to the results, all binders reached their final setting time during the 6 h-precuring period (360 min). The reductions (%) in the initial and final setting times due to the addition of the seeds and binary antifreeze admixture were comparable. Moreover, the experimental results showed that the maximum differences between initial and final setting times of around 50 min and 40 min were reported in C0 and C0AF, respectively. This time difference decreased by 40% in the seeded samples with/without the binary antifreeze admixture when compared to C0, regardless of the C–S–H seed content. This indicates the accelerated hydration rates of the binders prepared with seeds and antifreeze admixture.

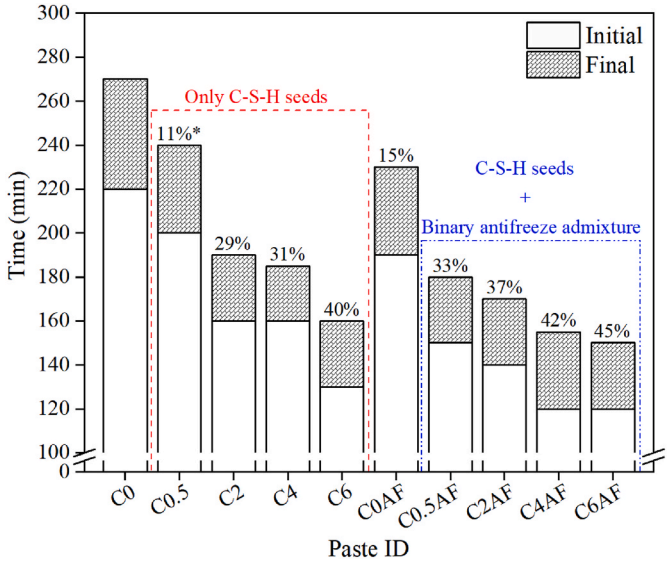

Fig. 4. Impacts of C–S–H seed content and the addition of the binary antifreeze admixture on the initial and final setting times of the binders at 23 ± 1 °C. (*Percentages indicate the reduction in the final setting time compared to C0).

Regarding the results, the final setting times of C0.5, C2, C4, and C6 were shortened by 11% (240 min), 29% (190 min), 32% (185 min), and 40% (160 min), respectively, when compared with C0 (270 min). This shows the more drastic early hydration process with increased seed content in the binders. Moreover, C0AF exhibited a 40 min (15%) earlier final setting time than that measured in C0. The latter can be attributed to the accelerated hydration of cement in the presence of calcium nitrate. Moreover, the early precipitation of NO_3-AFt can accelerate the formation of an interconnected AFt network that consumes a large portion of mixing water, which leads to the sudden loss of C0AF paste plasticity and rapid hardening, thereby accelerating the setting time [65]. Furthermore, the mutual accelerating impacts of C–S–H seeds and binary antifreeze admixture on setting time were more significant than only one additive (i.e., either seeds or antifreeze admixture). Therefore, the reductions in the final setting time increased to around 33% (180 min), 37% (170 min), 42% (155 min), and 45% (150 min) in C0.5AF, C2AF, C4AF, and C6AF, respectively, as compared to C0.

3.2. Freezing point and frozen water content

The freezing points and the amounts of frozen water (i.e., free water during the hydration) were decreased with increasing C–S–H seed content, precuring, and, more significantly, the addition of the binary antifreeze admixture (Figs. 5 and 6). The measured freezing points corresponding to each paste recipe are listed in Table 4. Based on the Clausius-Clapeyron relation and Raoult's law, the freezing point of the solution decreased with increasing ion concentration"concentration effect" [66,67]. The latter explains the lower freezing point of the C0-(0 h) pore solution (−1.3 °C) as compared to that of pure water (0 °C) due to dissolved ions from cement particles.

According to the results, the addition of C–S–H seeds slightly affected the freezing points in the absence of precuring, and the values ranged between −1.8 °C and −2.8 °C and decreased with increased seed content. The latter can be attributed to the enhanced very early dissolution of the cement particles (i.e., a higher number of ions released into pore solution) in the presence of C–S–H seeds, as reported previously [35,38]. On the other hand, the freezing points of the pastes decreased sharply with the addition of the binary antifreeze admixture due to the increased ions concentration in the mixing solution upon the dissolution of the antifreeze admixtures [8]. For instance, the freezing point decreased to as low as −10.2 °C in C0AF-(0 h). Moreover, the combination of C–S–H seeds and the binary antifreeze admixture further decreased the freezing point due to their mutual effects, so the freezing point of C6AF-(0 h) decreased to −11.1 °C.

Furthermore, the freezing point was further depressed with a short precuring period under room conditions. The impacts of precuring on the freezing point were more noticeable in the binders modified with C–S–H seeds and/or antifreeze admixture as compared to the control binder (C0). Therefore, the freezing point of the C6 binder decreased from −2.8 °C to −5.2 °C after the 6 h precuring, whereas an insignificant change in the freezing point was noted in C0-(6 h) after the precuring interval due to its slow early reaction rate reactivity. as shown in Fig. 3a. On the other hand, the freezing points of C0AF and C6AF decreased by 2.4 °C and 4 °C, respectively, after the 6 h precuring period.

During the precuring period at 23 ± 1 °C, the reactivity of cement was accelerated with both C–S–H seeds and the binary antifreeze admixture (as shown in Fig. 3, in Section 3.1.1). This resulted in the rapid consumption of free water with ongoing hydration (see Fig. 6) (i.e., decreased pore size [38]) and the accelerating formation of the hydration products network (as will be shown below in Sections 3.3).

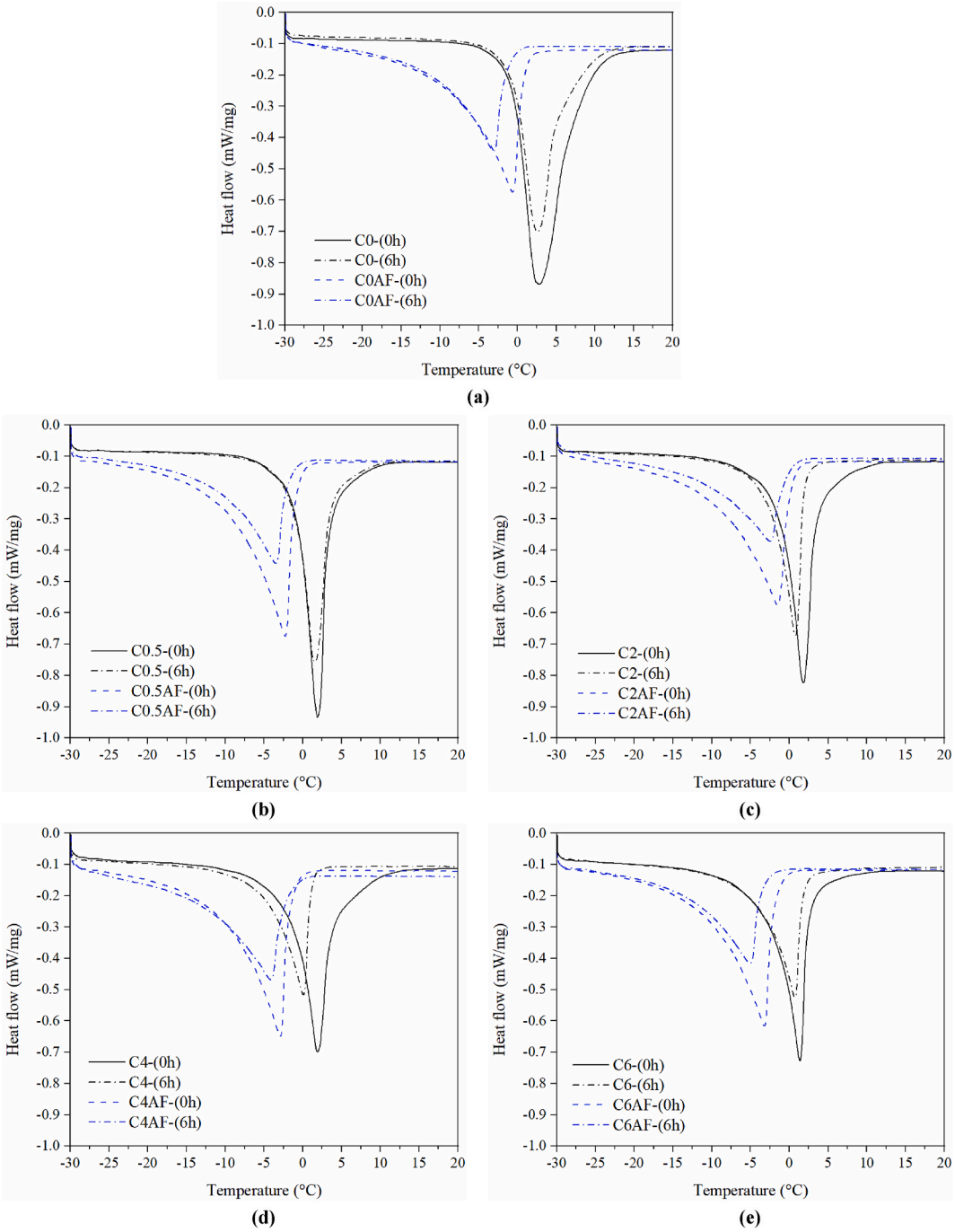

Fig. 5. LT-DSC heat flow curves of (a) C0 and C0AF; (b) C0.5 and C0.5AF; (c) C2 and C2AF; (d) C4 and C4AF; (e) C6 and C6AF with 0 h and 6 h precuring periods.

According to the literature [38,68–71], the freezing point of the pore solution in porous materials (i.e., cement paste in this study) decreased with decreased pore radius, or the "network effect" (Equation (5)).

$$\Delta T = -47/r \quad (5)$$

where ΔT is the change in freezing temperature and r is the pore radius in nanometers.

Fig. 6 shows the positive impacts of C–S–H seeds, precuring, and the binary antifreeze admixture in terms of decreasing the melting heat (i.e., frozen water amount). Regarding the results, C0-(0 h) exhibited the highest melting heat at around 62 J/g. This indicates the low consumption rate of mixing water due to its limited hydration progress with the 6 h precuring condition (as depicted previously in Fig. 3). The decreased melting heat in C0AF-(0 h) (53 J/g) as compared to C0-(0 h) also confirms the acceleration impact of the binary antifreeze admixture on the hydration rate of the cement. In addition, the amount of frozen water was further decreased to 51 J/g and 45 J/g in C6-(0 h) and C6AF-(0 h), respectively. This confirms that the reduction of the amount of frozen water, as compared to C0-(0 h), is more obvious with the use of the combined additives (i.e., C–S–H seeds and antifreeze admixture). Furthermore, the frozen water content decreased significantly after the 6 h precuring and more substantially in the seeded and admixed binders. For instance, the melting heat of C6-(0 h) and C6AF-(0 h) decreased by around 20.5 J/g and 16.7 J/g, respectively, after the 6 h precuring, while C0-(0 h) decreased by only 6.1 J/g. The significant decrease in the frozen water content in the pastes prepared with the seeds and antifreeze admixture and treated by precuring is mainly associated with

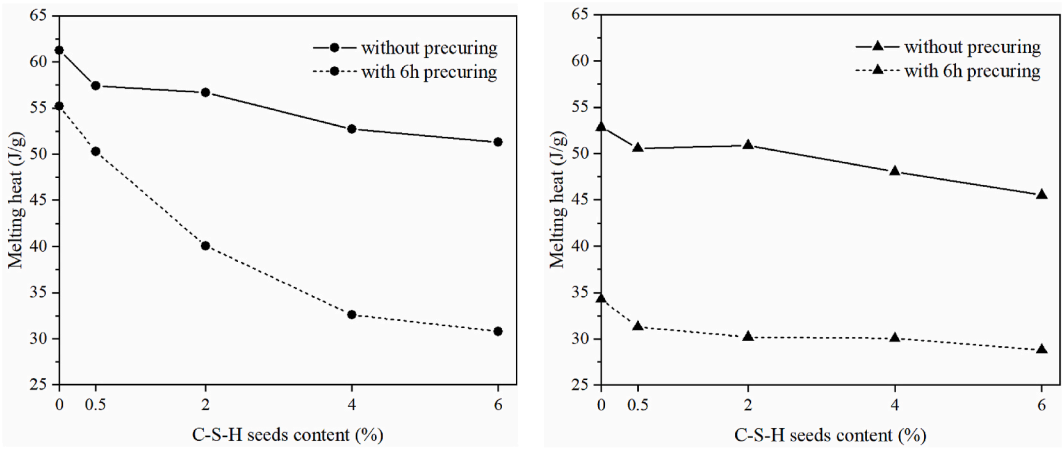

Fig. 6. Impacts of C–S–H seed content and room temperature 6 h precuring on melting heat (i.e., the amount of frozen water) of the binders: (a) without the binary antifreeze admixtures and (b) with the binary antifreeze admixtures.

Table 4
Freezing points of the binders with different precuring periods (°C).

Precuring period (h)	C0	C0AF	C0.5	C0.5AF	C2	C2AF	C4	C4AF	C6	C6AF
0	−1.3	−10.2	−1.8	−10.1	−1.6	−11.0	−2.1	−11.0	−2.8	−11.1
6	−1.6	−12.1	−1.9	−11.0	−1.2	−12.4	−4.7	−15.2	−5.2	−15.1

accelerated early hydration and, thereby, faster water consumption on the part of the precipitated hydration products during the 6 h precuring at 23 ± 1 °C. These findings are in line with the literature [8,38].

3.3. Hydration evolution

3.3.1. Hydration products

The impacts of 6 h precuring at room temperature, C–S–H seeds, and antifreeze admixture on the mineral phases consumption and formation of hydration products in C0, C6, C0AF, and C6AF cured at −10 °C are presented in Fig. 7. The consumption rate of C_2S, C_3S, and gypsum was accelerated with the precuring, C–S–H seeds, and addition of the binary antifreeze admixture. The latter confirms their positive impacts on the hydration reaction and indicates the reaction progress with time, even at −10 °C, which is consistent with the TGA/DTG results, as shown below in Fig. 8. Comparing the XRD patterns of the C0 and C6 samples, no change in the reaction products types was observed with the addition of C–S–H seeds. On the other hand, the inclusion of the binary antifreeze admixture in C0AF and C6AF led to the formation of NO_3-AFt and NO_3-AFm. Similar phases were previously observed in OPC-based materials mixed with calcium nitrate [60,72–75]. Choi et al. [60] and Balonis et al. [73] attributed the formation of NO_3-AFt to the accelerated reaction between NO_3^- and the C_3A cement phase, the incorporation of NO_3^- between the layers of the AFt layers, and the ion exchange between $SO_4^{2-}$and NO_3^-, whereas the formation of NO_3-AFm was mainly ascribed to the reaction between the early-forming NO_3-AFt and portlandite [60,72].

The amount of the hydration products increased (i.e., higher mass loss in TGA curves) with curing period, precuring, C–S–H seeds, and the addition of the antifreeze admixture, according to the TGA/DTG analysis (Fig. 8). Furthermore, the combined addition of the binary antifreeze admixture and C–S–H seeds, along with the 6 h precuring, further increased the amount of hydration products. It is worth mentioning that, due to the limited reactivity of C0-(0 h) and C6-(0 h) cured at −10 °C, their TGA/DTG curves were excluded.

Regarding the DTG curves of C0-(6 h) and C6-(6 h) [Fig. 8(a), and (b)], it is noticeable that the inclusion of C–S–H seeds favored the formation of C–S–H over portlandite ($Ca(OH)_2$) after the first curing day. This observation was more obvious in C0AF and C6AF, regardless of precuring condition. The lower peak intensity of the portlandite phase, as shown in the XRD patterns (see Fig. 7) of C–S–H seeds containing binders, supports these observations. Similarly, Huang and Yang [76] recently reported comparable observations. The reason behind this is still unclear, but it may be partially attributed to the decreased nucleation energy of C–S–H gel phase in the presence of C–S–H seeds, which accelerates the silicate hydration rate [77,78]. In addition, Sargam and Wang [5] proved that the presence of seeds can decrease the apparent energy of the C–S–H gel precipitation process, which facilitates the gel's precipitation-growth process. Furthermore, the precipitation of C–S–H gel is an autocatalytic reaction process [5]; thereby, the presence of the added C–S–H seeds in the pore solution can further stimulate the precipitation of C–S–H gel over the portlandite phase.

In addition, the formation of the NO_3-AFt and NO_3-AFm phase in C0AF and C6AF, regardless of the precuring condition, was further confirmed by TGA/DTG analysis. Balonis et al. [73] reported that the decomposition of nitrate hydrates occurs in three heating steps: (1) dehydration at around 110 °C (no separate peak can be detected here, due to the overlap with AFt, NO_3-AFt, and C–S–H peaks); (2) a reduction of NO_3^- to nitrite anion (NO_2^-) at 200–300 °C; and (3) the decomposition of NO_2^- at ≈520 °C. All decomposition peaks were observed in the DTG curves of the antifreeze admixture-containing mix compositions (Fig. 8(c), (d), (e), and (f)), demonstrating the precipitation of nitrate hydrates. Furthermore, a slight increase in calcite ($CaCO_3$) was noted in C0AF and C6AF, as compared to the C0 and C6 pastes. Upon the dissolution of urea in water, carbonic acid is produced [Equation (6)], which later reacts with $Ca(OH)_2$ according to Equation (7) to form calcite ($CaCO_3$). Choi et al. [60] and Wang et al. [45] reported strength enhancements in OPC-based mortar and concrete with the precipitation of NO_3-AFt and NO_3-AFm and calcite, respectively, due to their filling behavior. Therefore, the additional precipitated nitrate hydrates and calcite in this study may participate in densifying the microstructures and enhancing the mechanical and durability properties of C0AF and C6AF (as shown later in Sections 3.3.2, 3.4, and 3.5).

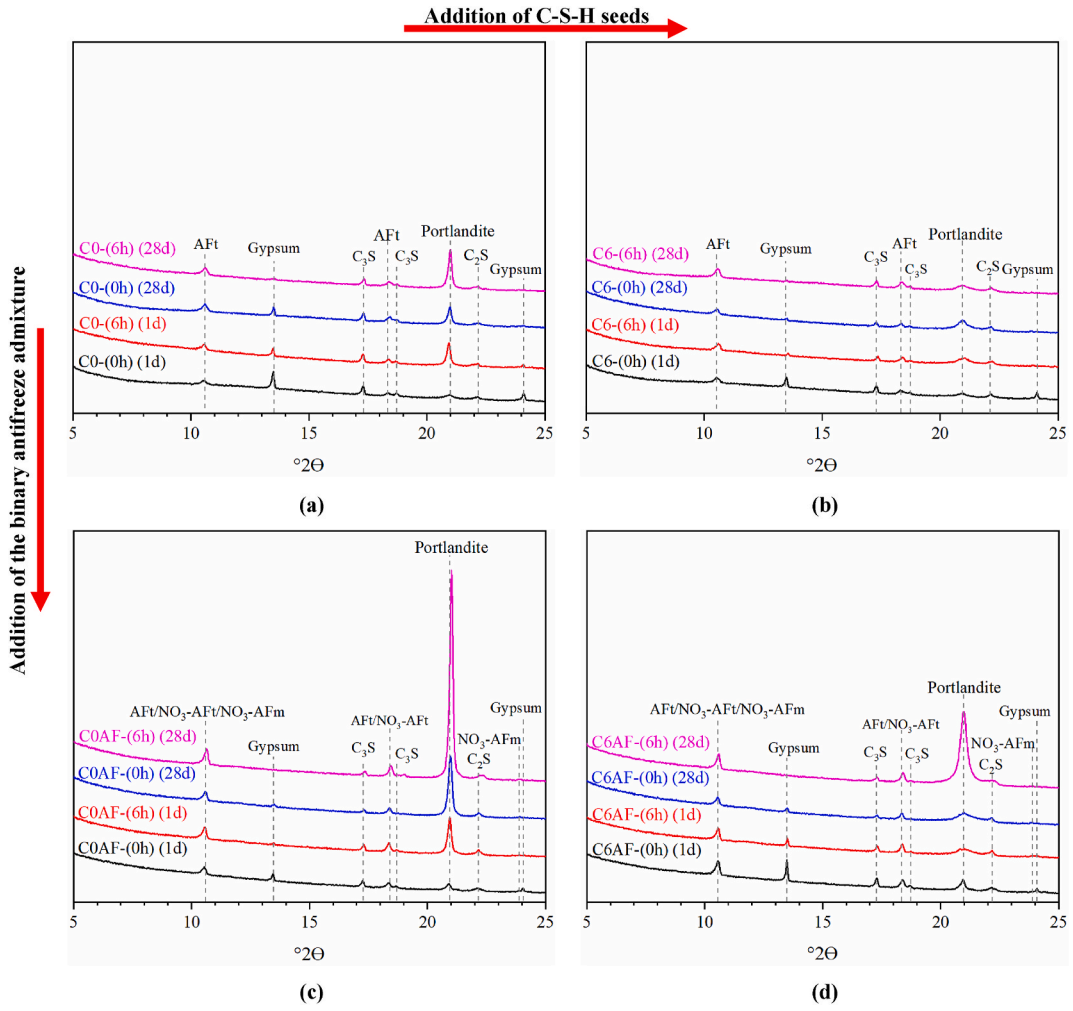

Fig. 7. The XRD patterns of 1 d and 28 d (with 0 h and 6 h-precuring) of: (a) C0; (b) C6; (c) C0AF; and (d) C6AF.

$$CO(NH_2)_2 + 2H_2O \rightarrow H_2CO_3 + 2NH_3 \quad (6)$$

$$H_2CO_3 + Ca(OH)_2 \rightarrow CaCO_3 + 2H_2O \quad (7)$$

Chemically bound water content can refer to the degree of hydration of cementitious binders. The lowest CBW content (<2%) was observed in the 28 d-old binders prepared without antifreeze admixture and precuring (i.e., C0-(0 h) and C6-(0 h); see Fig. 9). This is mainly attributed to the early freezing of these binders, and thus, a limited quantity of liquid-state free water was available for the hydration process (see Table 4 and Fig. 6(a)). On the other hand, the 6 h-precuring significantly increased the CBW content in C0-(6 h) and C6-(6 h) due to the accelerated and enhanced early hydration at 23 ± 1 °C. Therefore, CBW content increased to 3.1% and 4.9% and to 5.6% and 7.1% in the 1 d- and 28 d-old C0-(6 h) and C6-(6 h), respectively. The latter shows that the addition of C–S–H seeds amplified the beneficial impacts of precuring and, thus, improved the degree of hydration of the seeded binder (i.e., C6-(6 h)). This can be attributed to the nucleation and acceleration effects of the seeds embedded in the C6-(6 h) binder and the lower amount of frozen water (see Figs. 3 and 6(a)) when compared to C0-(6 h). Recently, Sargam and Wang [5] reported that the precipitation rate of hydration products in cementitious materials is proportional to the number of active nucleation/growth sites (i.e., C–S–H seeds in this study) available in pore solution. With the inclusion of the seeds, the hydration products preferentially grow on external C–S–H seeds; thereby, the nucleation of the newly formed phases should overcome less free energy, which facilitates and accelerates the precipitation process [46]. However, C0-(6 h) and C6-(6 h) exhibited a limited increase in CBW with time (Fig. 9(a)). This can be ascribed to the lack of free liquid-state water for the hydration process because of the freezing of a large portion of capillary water as a result of the higher freezing points of C0-(6 h) and C6-(6 h) as compared to the freezer curing temperature of this study (−10 °C) (see Table 4). Nevertheless, researchers previously reported that the freezing point of the pore solution trapped in nano-sized pores (<20 nm) can be as low as −40 °C, depending on pore diameter [79–82]. Subsequently, this supercooled pore solution may continue to dissolve cement particles and react with them in the small pores, resulting in a high-ion-concentration pore solution and additional hydration products. With ongoing hydration, the highly concentrated ions unfrozen pore solution in its small pores begin to migrate to ice-bodies in large pores until an equilibrium is reached [81,83,84]. As a result, ice in larger pores will start to melt due to increased ion concentration (Clausius-Clapeyron relation [67] and Raoult's law [66]). The latter can explain the limited increase in CBW with time in the frozen pastes (i.e., C0-(6 h) and C6-(6 h)).

The addition of the binary antifreeze admixture further increased the CBW content of the binders cured at −10 °C with or without precuring. Therefore, CBW content increased up to around 7.6% in 28 d-old C0AF-(0 h) and C6AF-(0 h). With the addition of the antifreeze admixture, the freezing points of the mixing water were drastically depressed, as shown in Section 3.2, and thereby, more liquid-state water was available for hydration. Furthermore, the increased CBW content can be also attributed to the acceleration and enhancement impacts of $Ca(NO_3)_2$ on the reactivity of OPC, as shown in Section 3.1 and reported previously [58,

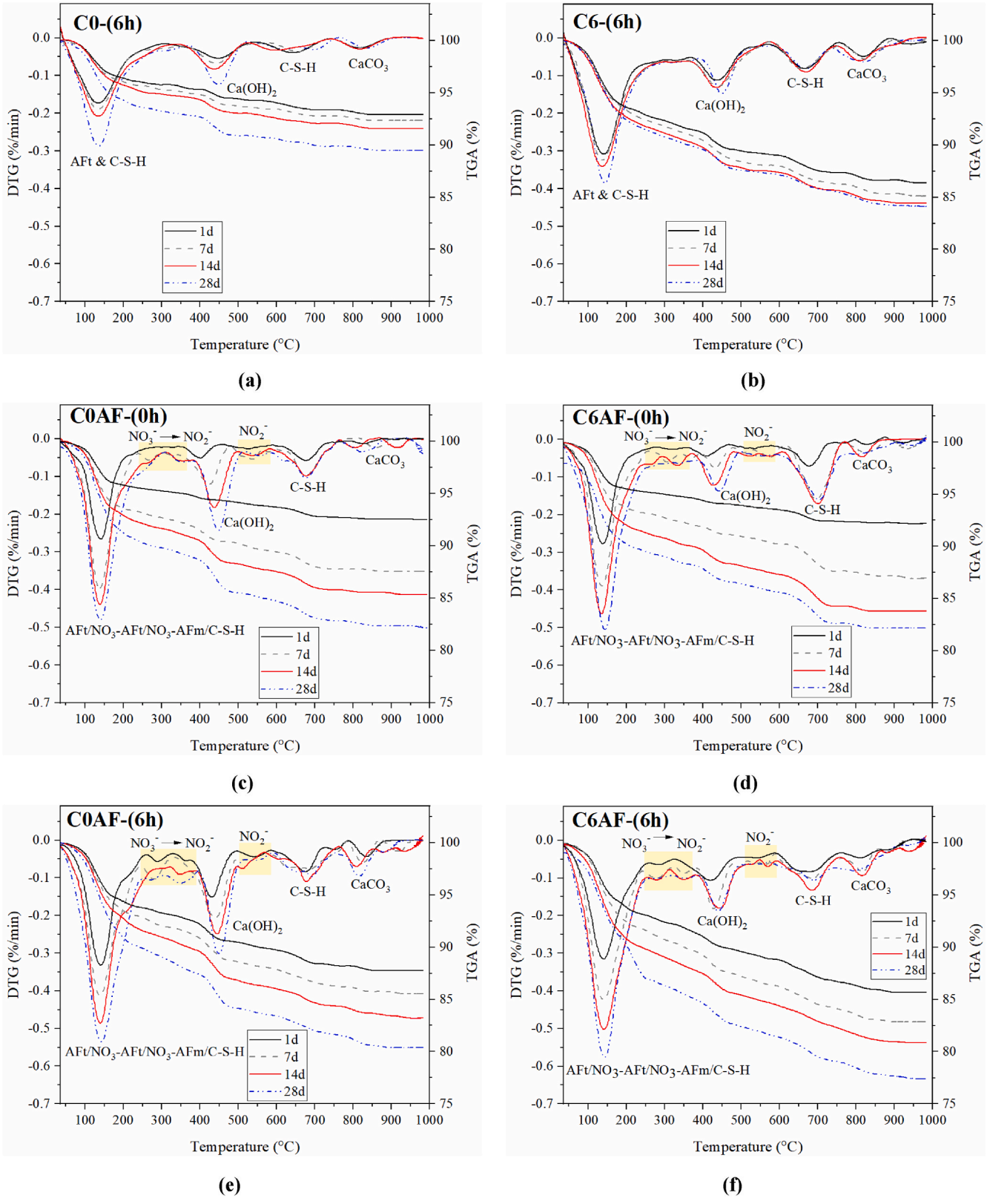

Fig. 8. TGA/DTG curves of the samples (a) C0-(6 h); (b) C6-(6 h); (c) C0AF-(0 h); (d) C6AF-(0 h); (e) C0AF-(6 h); and (f) C6AF-(6 h).

59,61]. With the 6 h precuring, the CBW of the binders was further improved, and the enhancements were more noticeable with the inclusion of C–S–H seeds. Thus, CBW increased by around 41% and 13.2% and around 42% and 21% in 1 d- and 28 d-old C0AF-(6 h) and C6AF-(6 h) when compared to their pairs without precuring, respectively.

3.3.2. *Microstructure*

In the absence of precuring and antifreeze admixture, long and connected cracks are observable in SEM images of the OPC pastes, regardless of the addition of C–S–H seeds (Fig. 10(a), (b)). This is because of the early and rapid freezing of mixing water in the fresh

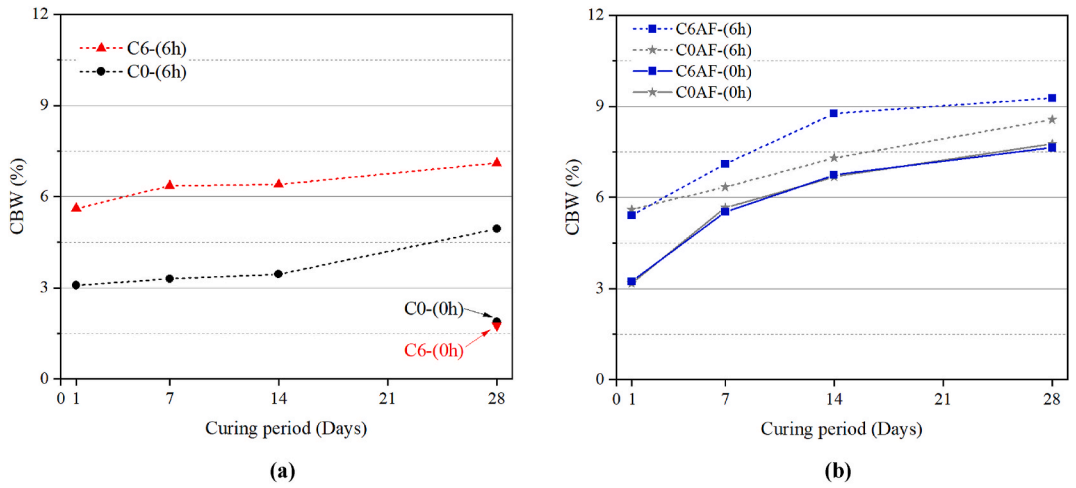

Fig. 9. The change in the content of chemically bound water (CBW) with time in the pastes: (a) without the binary antifreeze admixture and (b) with the binary antifreeze admixture.

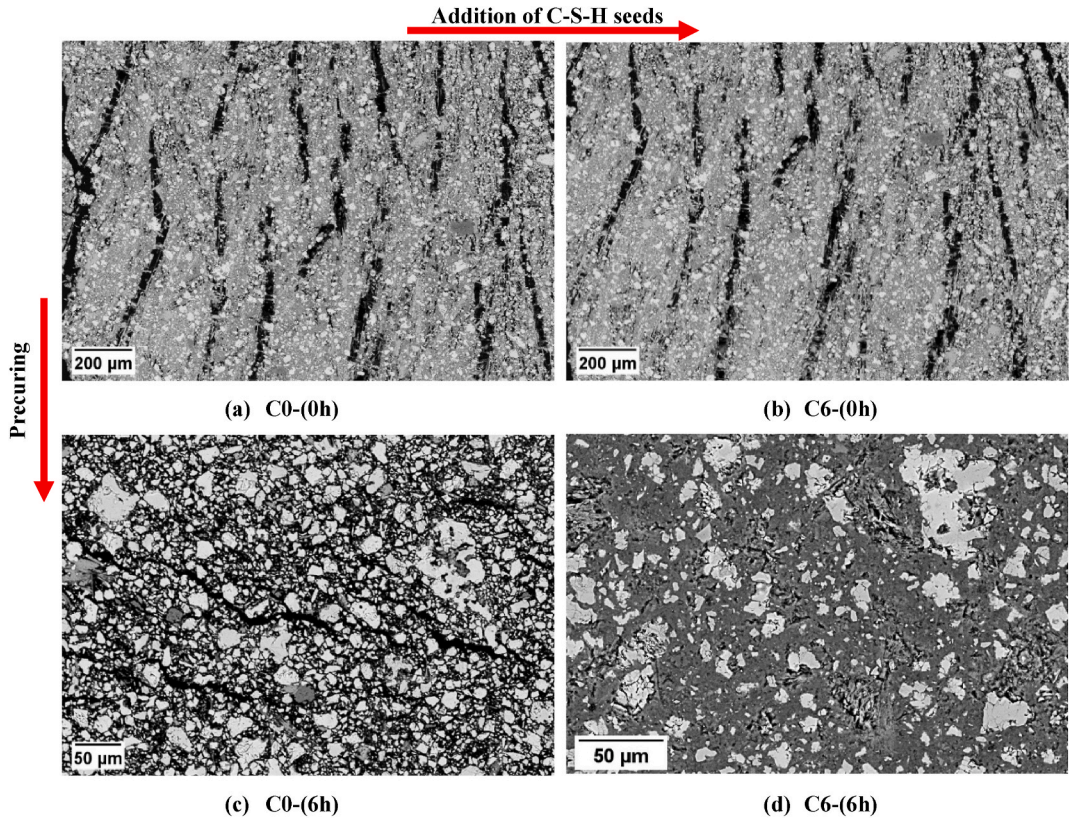

Fig. 10. Impacts of C–S–H seeds and precuring on the microstructures of 28 d-old hardened pastes cured at −10 °C. Light grey areas (unreacted OPC), textured grey areas (hydration products matrix), and black areas (cracks and voids). The time between parentheses indicates the precuring period.

pastes and the volume growth of ice crystals. With the 6 h precuring (Fig. 10(c), (d)), the microstructures become denser, with more precipitated hydration products in the pore solution. In comparison with C0-(6 h), the microstructure of C6-(6 h) was denser due to the enhanced early reactivity of the cement in the presence of C–S–H seeds, whereas C0-(6 h) was more prone to frost damage as compared to C6-(6 h) due to the higher amount of freezable free water in the pore structure (as shown in Fig. 6(a)). Moreover, due to the limited reaction progress in C0-(6 h) during the 6 h precuring (as shown in Fig. 3), it developed a weak hydration product network, which was not able to withstand the frost damage induced by the subsequent subzero curing condition (Fig. 10 (c)). Thus, a loose microstructure with extensive microstructural frost damage was captured in the 28 d C0-(6 h) paste. On the other hand, the addition of C–S–H seeds in C6-(6 h) accelerated the formation of a dense skeleton that was able to restrict the growth of ice crystals and withstand the increased internal hydraulic stress exerted on pore walls because of the volume expansion of ice crystals.

With the incorporation of the binary antifreeze admixture (Fig. 11), the microstructure compactness was enhanced, more significantly so when combined with C–S–H seeds and precuring. Large freezing defects (such as those observed in Fig. 10(a), (b)) were not detected in C0AF and C6AF, regardless of the precuring period, because of their lower freezing

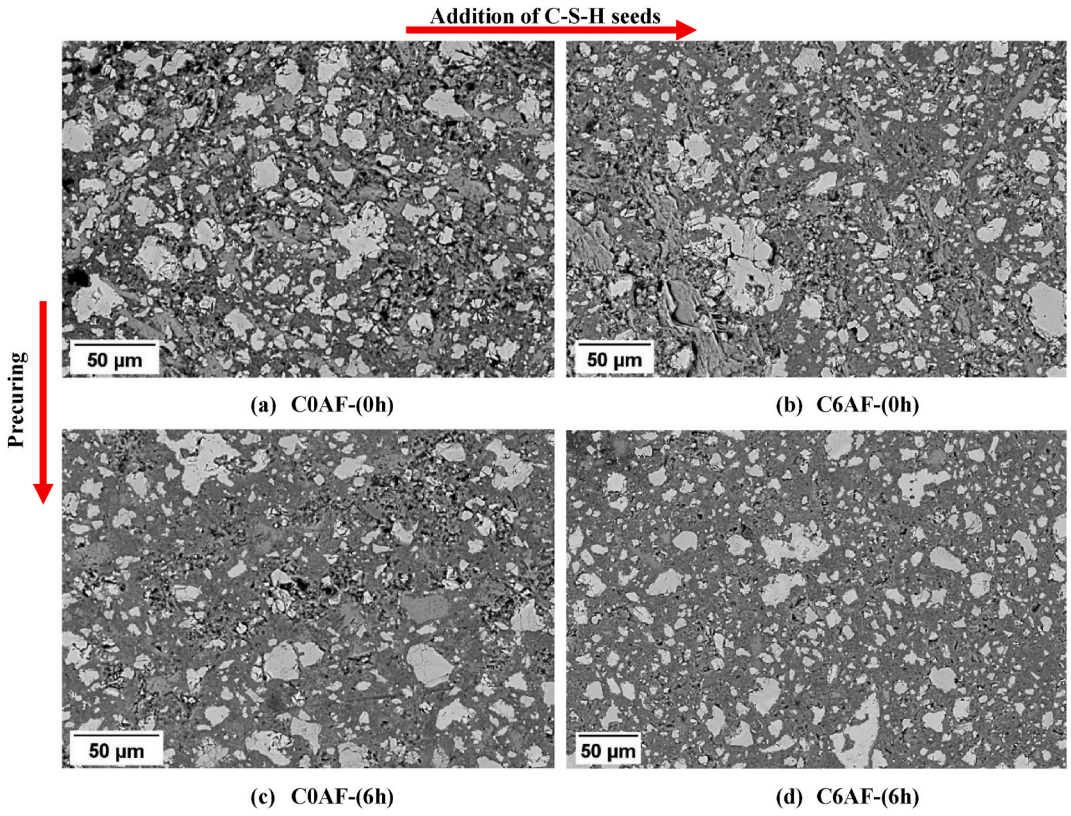

Fig. 11. Influences of 6 h precuring and C–S–H seeds on the microstructure compactness of 28 d-old pastes prepared with the binary antifreeze admixture.

points (see Table 4) as compared to the subzero curing temperature (i.e., −10 °C). Nevertheless, the absence of precuring resulted in loose microstructures with more distributed voids in C0AF-(0 h) and C6AF-(0 h) (Fig. 11(a), (b)), regardless of the addition of the seeds. The latter can be ascribed to the slow hydration rate at −10 °C and, thereby, the low hydrate precipitation rate. However, upon the adoption of the 6 h precuring treatment, the microstructures of C0AF-(6 h) and C6AF-(6 h) were significantly densified (Fig. 11(c), (d)). Because of the beneficial synergic impacts of the binary antifreeze admixture, C–S–H seeds, and precuring on the overall reaction degree of the system (as shown in Fig. 9(b)), C6AF-(6 h) exhibited a denser microstructure than C0AF-(6 h). The microstructural observations prove the effectiveness of the combination of binary antifreeze admixture, C–S–H seeds, and precuring on the compressive strength and durability properties of the pastes (as will be shown in Sections 3.4 and 3.5).

3.4. Strength development

Regardless of the content of C–S–H seeds, all subzero cured paste samples synthesized with the binary antifreeze admixture showed an increase in compressive strength with time, reaching a maximum of around 15 MPa in the 28 d-old C6AF (Fig. 12), whereas a value of 78 MPa was measured in the 28 d-old control paste (i.e., C0) cured at room temperature. Therefore, it is obvious that the subzero curing significantly slowed strength development. Moreover, all pastes without antifreeze admixture and 6 h precuring gained less than 5 MPa, even after 28 d, regardless of C–S–H seeds content, which can mainly be attributed to their early freezing. Therefore, the strength developments of the latter mixes were excluded from this study.

The strength development of subzero-cured pastes was significantly accelerated with a short period of precuring, and the strength enhancement was more obvious with the presence of C–S–H seeds (Fig. 13). Thus, the 1 d compressive strength increased to around 5.0, 9.7, 12.3, 17.8, and 19.7 MPa in C0-(6 h), C0.5-(6 h), C2-(6 h), C4-(6 h), and C6-(6 h), respectively, while no strength was gained in C0-(0 h) (Fig. 13(a)). Moreover, the impacts of 6 h precuring on strength development were more significant in the mutual presence of the seeds and binary antifreeze admixture (Fig. 13(b)). Therefore, the 1 d-old C0AF-(6 h), C0.5AF-(6 h), C2AF-(6 h), C4AF-(6 h), and C6AF-(6 h) cured at −10 °C showed compressive strengths increases of 10.2, 19.2, 21.7, 23.7, and 26.2 MPa, respectively. Furthermore, the beneficial impacts of C–S–H seeds and the binary antifreeze admixture on the 6 h-precured

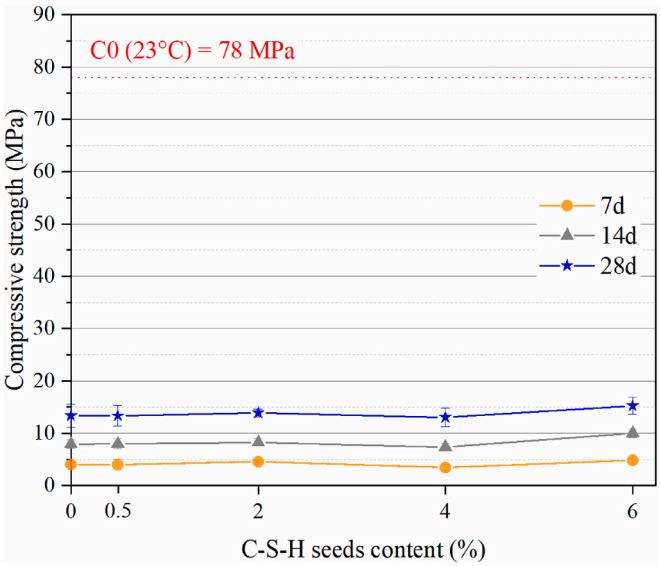

Fig. 12. Effects of C–S–H seeds on strength development of the binders prepared with the binary antifreeze admixture and cured at −10 C without precuring.

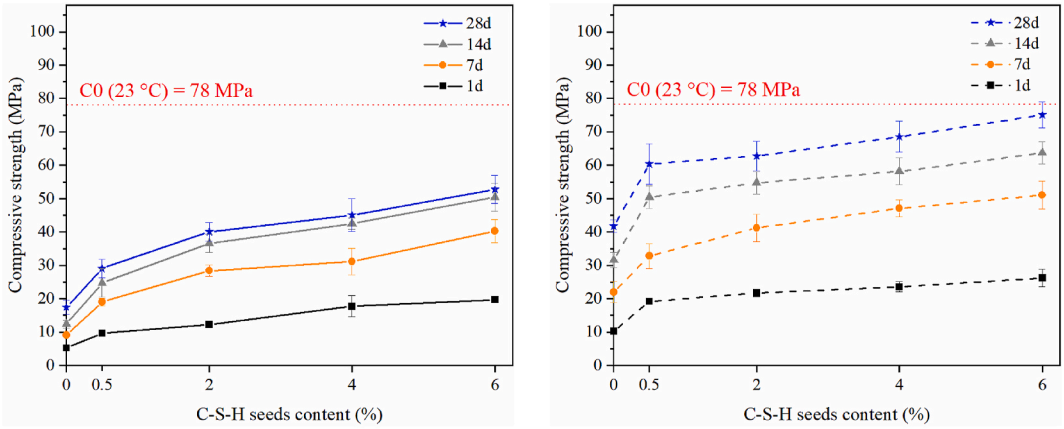

Fig. 13. Impacts of C–S–H seed content on 6 h-precured paste samples prepared (a) without the binary antifreeze admixture and (b) with the binary antifreeze admixture on strength development, as compared to the compressive strength of the 28 d-old control paste cured at room temperature (dotted line).

samples were also obvious at a late age (i.e., 28 d). Therefore, the 28 d-old C0AF-(6 h), C6-(6 h), and C6AF-(6 h) samples registered higher compressive strengths of around 41.7, 52.7, and 75.1 MPa, respectively, as compared to the 17.5 MPa measured in 28 d-old C0-(6 h). Promisingly, the 28-d compressive strength of C6AF-(6 h) was 96% of that measured in the 28 d-old control paste cured at room temperature. This highlights the real potential to extend the construction season in northern regions with lower demand for heating systems (i.e., lower CO_2 emissions, as shown below in Section 3.6). The reported strength enhancements are mainly attributed to the lower freezing points and frozen water content (Table 4 and Fig. 6), the nucleation effects of the embedded seeds (i.e., the faster precipitation of hydration products (Fig. 8), the development of dense microstructures (see Figs. 10 and 11), and the acceleration effect of $Ca(NO_3)_2$. Similarly, several studies previously reported an increase in compressive strength with the inclusion of C–S–H seeds and $Ca(NO_3)_2$ [37,38,59,85,86].

The normalized compressive strengths of the precured paste samples were given by the ratio $\left(\frac{f_c \text{ of mix composition paste}}{f_c \text{ of C0}-(6h)}\right)$, where f_c is the compressive strength, and the results are depicted in Fig. 14. With time, the compressive strengths of the precured samples were enhanced, and thus, 7 d-old C0AF-(6 h) was able to gain 2.5 times the compressive strength (22 MPa) of that (9 MPa) measured in C0-(6 h) of the same age, whereas the 7 d-old C6-(6 h) and C6AF-(6 h) pastes achieved around 4.5 and 5.7 times the compressive strength (40.3 and 51.1 MPa), respectively, of that gained in 7 d-old C0-(6 h). Worth mentioning that optimal C–S–H seeds dosage needs to be determined upon any change in binder composition, curing temperature, and w/c ratio to ensure the highest enhancements in the compressive strength and hydration degree of subzero-cured cementitious material.

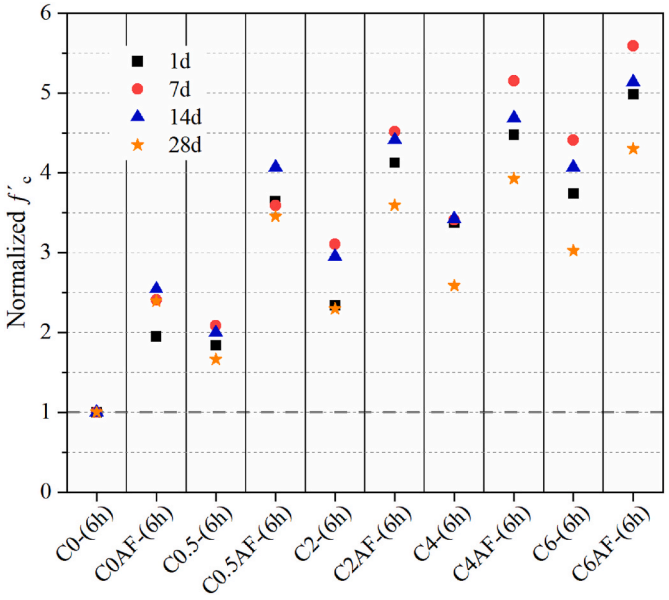

Fig. 14. Normalized compressive strength (f'_c) of the pastes.

3.5. Water absorption and permeable porosity

Water absorption and permeable porosity showed a decreasing trend with C–S–H seed content, precuring, and the usage of the binary antifreeze admixture (Fig. 15). The maximum water absorption (≈20%) and permeable porosity (≈35%) were measured in all paste samples without precuring and antifreeze admixture, regardless of C–S–H seed content (Fig. 15(a)), whereas the control paste (i.e., C0) cured at room temperature exhibited a water absorption and permeable porosity of around 4.3% and 6.9%, respectively (see Fig. A.1 in Appendix). This shows the destructive impacts of the subzero curing condition and the freezing of the pore solution on the microstructure's compactness and permeability, thereby easing the ingress of liquids from the surrounding (i.e., water in this study). However, because of the 6 h precuring, the water absorption and permeable porosity of C0-(6 h) decreased by up to 14.4% and 27.4%, respectively, when compared to C0-(0 h). With the mutual effects of C–S–H seeds and precuring, the reductions in water absorption and permeable porosity were more significant. Therefore, the water absorption and permeable porosity of C6-(6 h) decreased by 74.2% and 72.4%, respectively, as compared to those measured in the C0-(0 h). These results are in line with microstructural observations in Sections 3.3.2. It is worth noting that, despite the inclusion of C–S–H seeds and the provision of precuring in C6-(6 h), the water absorption (≈5.2%) and permeable porosity (≈9.7%) were still slightly higher than those measured in the control paste cured at room temperature.

Furthermore, the usage of the binary antifreeze admixture was very effective in limiting the water absorption and decreasing the permeable porosity, regardless of C–S–H addition and precuring (Fig. 15(b)). The latter can be assigned to the ability of the used binary antifreeze admixture to protect the pastes against freezing, thus eliminating the microstructural frost damage and minimizing the connectivity of the pores (as shown in Fig. 11) with the aid of the low w/c ratio (i.e., 0.27) employed in this study.

In line with the literature [50], the standard drying temperature (105 °C) drastically increased the measured water absorption and

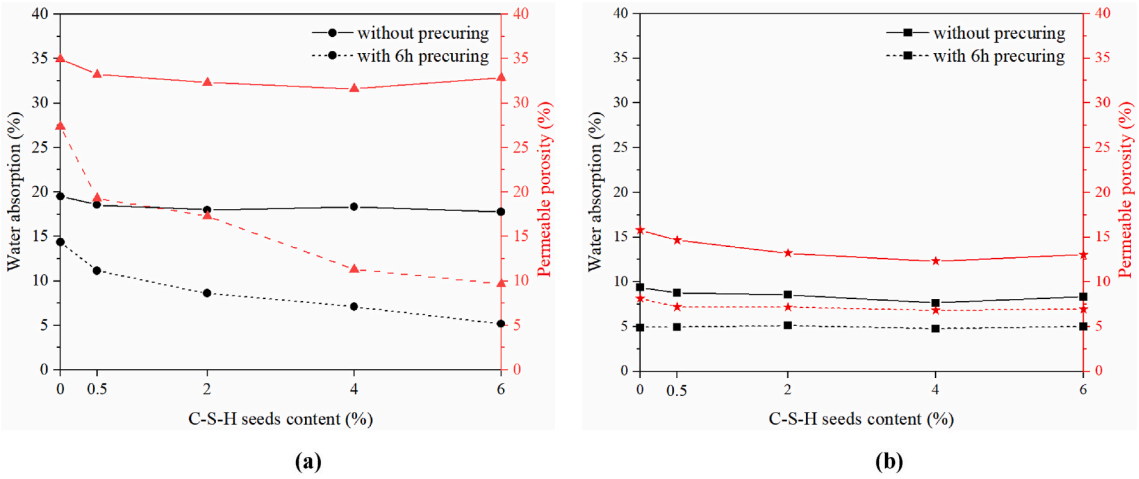

Fig. 15. Water absorption and permeable porosity of the 28 d-old pastes (a) without the binary antifreeze admixture and (b) with the binary antifreeze admixtures.

permeable porosity of the pastes (see Fig. A.1 in Appendix). The latter can be attributed to the dehydration of ettringite (see Fig. A.2) and the partial dehydration of C–S–H gel at 105 °C. Similarly, Thériné et al. [50] showed that a high drying temperature (>30 °C) removes a portion of CBW from hardened cement paste as a result of ettringite dehydration, thereby increasing both porosity and water absorption.

3.6. Environmental assessment

Based on the compressive strength development of the OPC-based binders at −10 °C, it was demonstrated that the needed heating system operating time to achieve comparable room temperature compressive strength at −10 °C can be significantly shortened to only 6 h via the mutual addition of 6 wt% C–S–H seeds and the binary antifreeze admixture (see Fig. 13(b)) whereas the 28 d-old C0-(6 h) cured at −10 °C was able to gain only 25% of the compressive strength gained by the 28 d-old C0 cured at room temperature. Thus, the C0 mix cured at −10 °C must be protected against the subzero ambient temperature and maintained at 23 ± 1 °C for the entire 28 d to gain a compressive strength comparable to that of C0 cured at room temperature. Thereby, the operating time of the heating system was set at 672 h (≈28 d) and 6 h for C0 and C6AF mix compositions, respectively.

To assess the environmental benefits of using the C6AF mix composition in winter construction works, a direct frame-work heating technique was adopted in this study instead of a heated shaded area, which is known for its high heat loss to the surroundings [87]. The calculation was performed using a diesel-fueled hydronic heating system (90–94% heat efficiency) and traditional plywood in 21 mm thick sheets, with a thermal conductivity and heat transfer resistance of around 0.14 W/mK and 0.15 m^2K/W, respectively. A diesel energy content of 9.7 kWh/L and CO_2 emissions of 2.7 kg/L were considered in the calculations. To simplify the calculations, a framework wall side area of 1 m^2 was adopted for the calculation of the heat energy needed to maintain the temperature at 23 ± 1 °C throughout the framework when the ambient temperature is −10 °C using Equations (8) and (9) [88].

$$q = U \times A \times dT \quad (8)$$

$$U = {}^{1}/_{R} \quad (9)$$

where q is heat transfer (W), U is the overall heat transfer coefficient (W/m^2K), A is the wall area (m^2), dT is the temperature difference over the wall, and R is the heat transfer resistance (W/m^2K).

A significant decrease in the required heat energy and CO_2 was calculated when C6AF was employed in place of C0 at −10 °C ambient temperature for the same 28 d compressive strength (Table 5).

Table 5
The consumed heat energy and related CO_2 emissions by the used heating system at a −10 °C ambient temperature.

Mix composition	Total heat energy (kWh/m^2)	CO_2 emission (kg/m^2)
C0	148.8	47.7
C6AF	1.3	0.4

Therefore, the total required heat energy of C6AF is 0.9% that needed for C0. Similarly, the CO_2 emissions decreased from 47.7 kg to 0.4 kg for each 1 m^2 of the framework. It is worth noting that these calculations did not consider the hydration heat and potential impacts of concrete element volume in practical application, which may shorten the required heating period for C0. Nevertheless, the potential to lower the energy consumption and CO_2 emissions during winter construction activities via the incorporation of C–S–H seeds and binary antifreeze admixtures is obvious. The findings of this study indicate the real potential to extend the construction season in northern regions and lower energy consumption and CO_2 emissions, accompanied with comparable mechanical and durability properties as those gained at standard curing conditions.

4. Conclusion

This study aims to develop a binder via which the construction season in northern regions can be extended, with a lower demand for heating systems. The mutual effect of C–S–H seeds, binary antifreeze admixture (i.e., urea and calcium nitrate), and short interval precuring at room temperature on ordinary Portland cement (OPC) binder are investigated.

The incorporation of the C–S–H seeds accelerates the hydration rate and setting time of OPC-based pastes during the 6 h-precuring, and the acceleration rate is directly proportional to seed content. The mutual presence of the seeds and the binary antifreeze admixture further accelerates hydration. The addition of the binary antifreeze admixture can lower the binder freezing point to below −10 °C, regardless of C–S–H seed content. The combined addition of C–S–H seeds, binary antifreeze admixture, and precuring can additionally depress the freezing points of the pastes to −15.1 °C. Simultaneously, the amount of frozen water is reduced as a result of the accelerated hydration rate and consumption of free water.

The pastes modified with the C–S–H seeds, binary antifreeze admixture, and precuring show a significantly higher amount of precipitated hydration products and chemically bound water as compared to the control paste when both were cured at −10 °C.

Furthermore, the microstructure assessment demonstrates the effectiveness of the combined addition of the seeds, binary antifreeze admixture, and precuring in terms of enhancing the microstructure's compactness and frost resistance. Promisingly, with 6 wt% C–S–H seeds, antifreeze admixture, and 6 h-precuring, the 28-d compressive strength of subzero cured paste can reach 75.1 MPa, which is 96% of the value measured in the control paste (78 MPa) cured at room temperature. The subzero curing temperature increases the water absorption and permeable porosity considerably. On the other hand, the addition of C–S–H seeds, antifreeze admixture, and precuring can drastically reduce them, resulting in comparable durability properties to those detected in the control paste cured at room temperature. The study demonstrates the importance of the room-temperature precuring period and its substantial effects on the efficiency of C–S–H seeds and binary chloride-free antifreeze admixture in accelerating the strength development of subzero-cured paste.

This study shows the real potential to extend the construction season in northern areas with lower energy consumption and CO_2 emissions.

Author contribution

Ahmad Alzaza: Conceptualization, Data curation, Formal analysis, Investigation, Methodology, Validation, Visualization, Writing – original draft, Writing – review & editing. **Katja Ohenoja:** Conceptualization, Methodology, Formal analysis, Validation, Visualization, Writing – review & editing, Supervision, Funding acquisition. **Isak Langås:** Validation, Writing – review & editing. **Bård Arntsen:** Validation, Writing – review & editing. **Minna Poikelispää:** Validation, Writing – review & editing. **Mirja Illikainen:** Conceptualization, Resources, Visualization, Writing – review & editing, Supervision, Funding acquisition.

Funding

This work was carried out under the auspices of the ARCTIC-ecocrete project, which is supported by Interreg Nord program funded by European Regional Development Fund and the Regional Council of Lapland.

Declaration of competing interest

The authors declare that they have no known competing financial interests or personal relationships that could have appeared to influence the work reported in this paper.

Acknowledgment

Mr. Jarno Karvonen and Mr. Tun Nyo are acknowledged for their contributions to the laboratory work. Mr. Håkan Nykvist (Master Builders Solutions, Sweden), Mr. Petri Manninen (Sika, Finland), and Mr. Esa Heikkilä (Finnsementti, Finland) are acknowledged for providing materials for this study. The authors thank the Centre for Material Analysis, University of Oulu, Finland.

Appendix

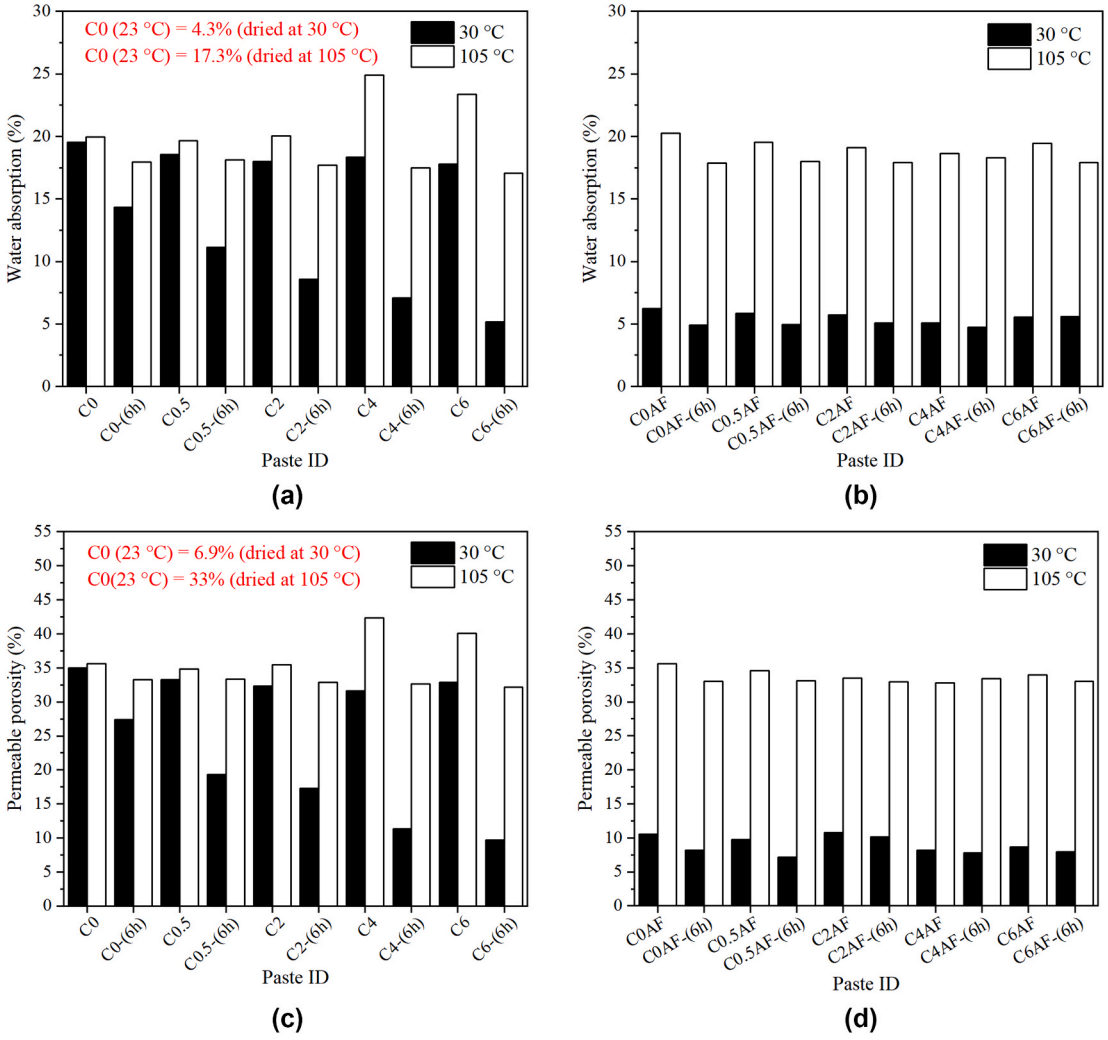

Fig. A.1. Impacts of drying temperature on the water absorption (a and b) and permeable porosity (c and d) of 28 d-old pastes.

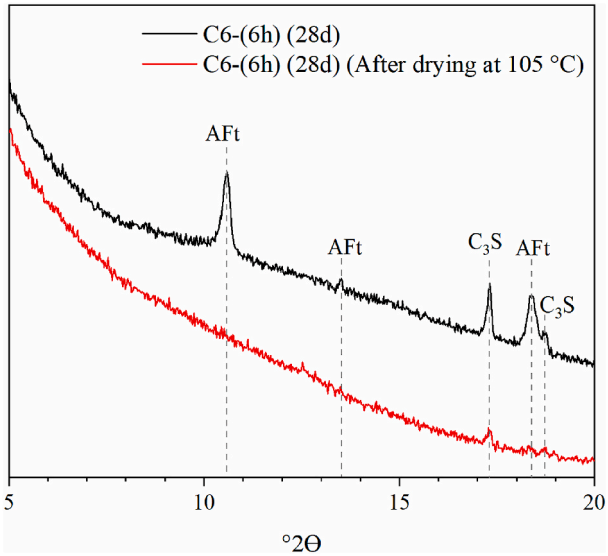

Fig. A.2. Impacts of drying step at 105 °C on ettringite phase in the 28 d-old C6-(6h) paste.

References

[1] ACI Committee, Guide to cold weather concreting "ACI 306R-10, Am. Concr. Inst (2010). Farmington Hills Mich. USA.

[2] J. Dai, Q. Wang, X. Lou, X. Bao, B. Zhang, J. Wang, X. Zhang, Solution calorimetry to assess effects of water-cement ratio and low temperature on hydration heat of cement, Construct. Build. Mater. 269 (2021) 121222, https://doi.org/10.1016/j.conbuildmat.2020.121222.

[3] H. Zhao, K. Jiang, Y. Di, W. Xu, W. Li, Q. Tian, J. Liu, Effects of curing temperature and superabsorbent polymers on hydration of early-age cement paste containing a CaO-based expansive additive, Mater. Struct. 52 (2019) 108, https://doi.org/10.1617/s11527-019-1407-0.

[4] L. Senff, D. Hotza, W.L. Repette, V.M. Ferreira, J.A. Labrincha, Mortars with nano-SiO2 and micro-SiO2 investigated by experimental design, Construct. Build. Mater. 24 (2010) 1432–1437, https://doi.org/10.1016/j.conbuildmat.2010.01.012.

[5] Y. Sargam, K. Wang, Hydration kinetics and activation energy of cement pastes containing various nanoparticles, Compos. B Eng. 216 (2021) 108836, https://doi.org/10.1016/j.compositesb.2021.108836.

[6] J.M. Nixon, A.K. Schindler, R.W. Barnes, S.A. Wade, Evaluation of the Maturity Method to Estimate Concrete Strength in Field Applications, 2008. https://trid.trb.org/view/850218. (Accessed 25 April 2021).

[7] D.P. Bentz, Activation energies of high-volume fly ash ternary blends: hydration and setting, Cement Concr. Compos. 53 (2014) 214–223, https://doi.org/10.1016/j.cemconcomp.2014.06.018.

[8] S. Zhang, Y. Zhao, H. Ding, J. Qiu, C. Hou, Effect of sodium chloride concentration and pre-curing time on the properties of cemented paste backfill in a sub-zero environment, J. Clean. Prod. 283 (2021) 125310, https://doi.org/10.1016/j.jclepro.2020.125310.

[9] J. Khan, S.K. G, Influence of binary antifreeze admixtures on strength performance of concrete under cold weather conditions, J. Build. Eng. 34 (2021) 102055, https://doi.org/10.1016/j.jobe.2020.102055.

[10] F. Karagol, R. Demirboga, W.H. Khushefati, Behavior of fresh and hardened concretes with antifreeze admixtures in deep-freeze low temperatures and exterior winter conditions, Construct. Build. Mater. 76 (2015) 388–395, https://doi.org/10.1016/j.conbuildmat.2014.12.011.

[11] A. Alzaza, K. Ohenoja, M. Illikainen, One-part alkali-activated blast furnace slag for sustainable construction at subzero temperatures, Construct. Build. Mater. 276 (2021) 122026, https://doi.org/10.1016/j.conbuildmat.2020.122026.

[12] G. Zhang, Y. Yang, H. Yang, H. Li, Calcium sulphoaluminate cement used as mineral accelerator to improve the property of Portland cement at sub-zero temperature, Cement Concr. Compos. 106 (2020) 103452, https://doi.org/10.1016/j.cemconcomp.2019.103452.

[13] G. Huang, D. Pudasainee, R. Gupta, W. Victor Liu, Hydration reaction and strength development of calcium sulfoaluminate cement-based mortar cured at cold temperatures, Construct. Build. Mater. 224 (2019) 493–503, https://doi.org/10.1016/j.conbuildmat.2019.07.085.

[14] P. Li, X. Gao, K. Wang, V.W.Y. Tam, W. Li, Hydration mechanism and early frost resistance of calcium sulfoaluminate cement concrete, Construct. Build. Mater. 239 (2020) 117862, https://doi.org/10.1016/j.conbuildmat.2019.117862.

[15] C.J. Korhonen, Antifreeze Admixtures for Cold Regions Concreting: a Literature Review, Cold Regions Research and Engineering Lab Hanover NH, 1990. https://apps.dtic.mil/sti/pdfs/ADA228559.pdf.

[16] R. Polat, The effect of antifreeze additives on fresh concrete subjected to freezing and thawing cycles, Cold Reg. Sci. Technol. 127 (2016) 10–17, https://doi.org/10.1016/j.coldregions.2016.04.008.

[17] A. Kicaite, The effect OF calcium nitrate ON the properties OF portland cement pastes and concrete hardening at low temperatures, Ceram. - Silik. (2020) 263–270, https://doi.org/10.13168/cs.2020.0015.

[18] C.J. Korhonen, Off-the-shelf Antifreeze Admixtures, Engineer Research and Development Center (ERDC), Cold Regions Research and Engineering Laboratory (CRREL), 2002. Hanover, New Hampshire, https://apps.dtic.mil/dtic/tr/fulltext/u2/a401312.pdf.

[19] R. Demirboğa, F. Karagöl, R. Polat, M.A. Kaygusuz, The effects of urea on strength gaining of fresh concrete under the cold weather conditions, Construct. Build. Mater. 64 (2014) 114–120, https://doi.org/10.1016/j.conbuildmat.2014.04.008.

[20] L.A. Barna, P.M. Seman, C.J. Korhonen, Energy-efficient approach to cold-weather concreting, J. Mater. Civ. Eng. 23 (2011) 1544–1551, https://doi.org/10.1061/(ASCE)MT.1943-5533.0000262.

[21] C. Korhonen, B. Charest, K. Romisch, Developing New Low-Temperature Admixtures for Concrete. A Field Evaluation, Defense Technical Information Center, Fort Belvoir, VA, 1997, https://doi.org/10.21236/ADA325475.

[22] T. Petersen, P.-L. Valdenaire, R. Pellenq, F.-J. Ulm, A reaction model for cement solidification: Evolving the C–S–H packing density at the micrometer-scale, J. Mech. Phys. Solid. 118 (2018) 58–73, https://doi.org/10.1016/j.jmps.2018.05.010.

[23] M. Sumesh, U.J. Alengaram, M.Z. Jumaat, K.H. Mo, M.F. Alnahhal, Incorporation of nano-materials in cement composite and geopolymer based paste and mortar–A review, Construct. Build. Mater. 148 (2017) 62–84, https://doi.org/10.1016/j.conbuildmat.2017.04.206.

[24] Y. Reches, Nanoparticles as concrete additives: review and perspectives, Construct. Build. Mater. 175 (2018) 483–495, https://doi.org/10.1016/j.conbuildmat.2018.04.214.

[25] K. Behfarnia, M. Rostami, Effects of micro and nanoparticles of SiO2 on the permeability of alkali activated slag concrete, Construct. Build. Mater. 131 (2017) 205–213, https://doi.org/10.1016/j.conbuildmat.2016.11.070.

[26] M. Oltulu, R. Şahin, Effect of nano-SiO_2, nano-Al_2O_3 and nano-Fe_2O_3 powders on compressive strengths and capillary water absorption of cement mortar containing fly ash: a comparative study, Energy Build. 58 (2013) 292–301, https://doi.org/10.1016/j.enbuild.2012.12.014.

[27] D. Siang Ng, S.C. Paul, V. Anggraini, S.Y. Kong, T.S. Qureshi, C.R. Rodriguez, Q. Liu, B. Savija, Influence of SiO2, TiO2 and Fe2O3 nanoparticles on the properties of fly ash blended cement mortars, Construct. Build. Mater. 258 (2020) 119627, https://doi.org/10.1016/j.conbuildmat.2020.119627.

[28] M. Aly, M.S.J. Hashmi, A.G. Olabi, M. Messeiry, A.I. Hussain, Effect of nano clay particles on mechanical, thermal and physical behaviours of waste-glass cement mortars, Mater. Sci. Eng. 528 (2011) 7991–7998, https://doi.org/10.1016/j.msea.2011.07.058.

[29] J. Björnström, A. Martinelli, A. Matic, L. Börjesson, I. Panas, Accelerating effects of colloidal nano-silica for beneficial calcium–silicate–hydrate formation in cement, Chem. Phys. Lett. 392 (2004) 242–248, https://doi.org/10.1016/j.cplett.2004.05.071.

[30] A. Nazari, S. Riahi, The effects of TiO_2 nanoparticles on physical, thermal and mechanical properties of concrete using ground granulated blast furnace slag as binder, Mater. Sci. Eng. 528 (2011) 2085–2092, https://doi.org/10.1016/j.msea.2010.11.070.

[31] A. Hosan, F.U.A. Shaikh, P. Sarker, F. Aslani, Nano- and micro-scale characterisation of interfacial transition zone (ITZ) of high volume slag and slag-fly ash blended concretes containing nano SiO2 and nano CaCO3, Construct. Build. Mater. (2020) 121311, https://doi.org/10.1016/j.conbuildmat.2020.121311.

[32] B.Y. Lee, K.E. Kurtis, Influence of TiO2 nanoparticles on early C3S hydration, J. Am. Ceram. Soc. 93 (2010) 3399–3405, https://doi.org/10.1111/j.1551-2916.2010.03868.x.

[33] G. Land, D. Stephan, Controlling cement hydration with nanoparticles, Cement Concr. Compos. 57 (2015) 64–67, https://doi.org/10.1016/j.cemconcomp.2014.12.003.

[34] P. Bost, M. Regnier, M. Horgnies, Comparison of the accelerating effect of various additions on the early hydration of Portland cement, Construct. Build. Mater. 113 (2016) 290–296, https://doi.org/10.1016/j.conbuildmat.2016.03.052.

[35] H.C. Pedrosa, O.M. Reales, V.D. Reis, M. das D. Paiva, E.M.R. Fairbairn, Hydration of Portland cement accelerated by C-S-H seeds at different temperatures, Cement Concr. Res. 129 (2020) 105978, https://doi.org/10.1016/j.cemconres.2020.105978.

[36] G. Land, D. Stephan, Preparation and application of nanoscaled C-S-H as an accelerator for cement hydration, in: K. Sobolev, S.P. Shah (Eds.), Nanotechnol. Constr., Springer International Publishing, Cham, 2015, pp. 117–122, https://doi.org/10.1007/978-3-319-17088-6_14.

[37] F. Wang, X. Kong, L. Jiang, D. Wang, The acceleration mechanism of nano-C-S-H particles on OPC hydration, Construct. Build. Mater. 249 (2020) 118734, https://doi.org/10.1016/j.conbuildmat.2020.118734.

[38] G. Zhang, Y. Yang, H. Li, Calcium-silicate-hydrate seeds as an accelerator for saving energy in cold weather concreting, Construct. Build. Mater. 264 (2020) 120191, https://doi.org/10.1016/j.conbuildmat.2020.120191.

[39] L. Nicoleau, G. Albrecht, K. Lorenz, E. Jetzlsperger, D. Fridrich, T. Wohlhaupter, R. Dorfner, H. Leitner, M. Vierle, D. Schmitt, M. Braeu, C. Hesse, S.M. Pancera, S. Zuern, M. Kutschera, Plasticizer-containing Hardening Accelerator Composition, US8653186B2, 2014. https://patents.google.com/patent/US8653186B2/en. (Accessed 1 April 2021). accessed.

[40] G.N. Lewis, G.H. Burrows, THE FREE ENERGY OF ORGANIC COMPOUNDS. I. THE REVERSIBLE SYNTHESIS OF UREA AND OF AMMONIUM CYANATE., (n.d.) 15.

[41] M. Ikeguchi, S. Nakamura, K. Shimizu, Molecular dynamics study on hydrophobic effects in aqueous urea solutions, J. Am. Chem. Soc. 123 (2001) 677–682, https://doi.org/10.1021/ja002064f.

[42] H.-Y. Kim, Urea additives for reduction of hydration heat in cement composites, Construct. Build. Mater. 156 (2017) 790–798, https://doi.org/10.1016/j.conbuildmat.2017.09.042.

[43] EN196-3, Methods for Testing Cement: Part 3. Determination of Setting Time and Soundness, CEN, Brussels, 2016.

[44] A. Damasceni, L. Dei, E. Fratini, F. Ridi, S.-H. Chen, P. Baglioni, A novel approach based on differential scanning calorimetry applied to the study of tricalcium silicate hydration kinetics, J. Phys. Chem. B 106 (2002) 11572–11578, https://doi.org/10.1021/jp0202111.

[45] L. Wang, S. Ju, H. Chu, Z. Liu, Z. Yang, F. Wang, J. Jiang, Hydration process and microstructure evolution of low exothermic concrete produced with urea, Construct. Build. Mater. 248 (2020) 118640, https://doi.org/10.1016/j.conbuildmat.2020.118640.

[46] F. Wang, X. Kong, L. Jiang, D. Wang, The acceleration mechanism of nano-C-S-H particles on OPC hydration, Construct. Build. Mater. 249 (2020) 118734, https://doi.org/10.1016/j.conbuildmat.2020.118734.

[47] S.M. Monteagudo, A. Moragues, J.C. Gálvez, M.J. Casati, E. Reyes, The degree of hydration assessment of blended cement pastes by differential thermal and thermogravimetric analysis. Morphological evolution of the solid phases, Thermochim. Acta 592 (2014) 37–51, https://doi.org/10.1016/j.tca.2014.08.008.

[48] A. Alzaza, K. Ohenoja, M. Illikainen, Enhancing the mechanical and durability properties of subzero-cured one-part alkali-activated blast furnace slag mortar by using submicron metallurgical residue as an additive, Cement Concr. Compos. (2021) 104128, https://doi.org/10.1016/j.cemconcomp.2021.104128.

[49] ASTM C642, Standard Test Method for Density, Absorption, and Voids in Hardened Concrete, 2006, ASTM International, West Conshohocken, PA, 2006. USA, www.astm.org.

[50] F. Thériné, E. Keita, J. Naël-Redolfi, P. Boustingorry, L. Bonafous, N. Roussel, Water absorption of recycled aggregates: measurements, influence of temperature

and practical consequences, Cement Concr. Res. 137 (2020) 106196, https://doi.org/10.1016/j.cemconres.2020.106196.
[51] W. Tian, B. Qi, Y. Liu, K. Liu, W. Wang, Early frost resistance and permeability properties of carbon fiber/cement-based composite cured by ohmic heating under ultra-low temperature, Construct. Build. Mater. 282 (2021) 122729, https://doi.org/10.1016/j.conbuildmat.2021.122729.
[52] M.H. Maciel, G.S. Soares, R.C. de O. Romano, M.A. Cincotto, Monitoring of Portland cement chemical reaction and quantification of the hydrated products by XRD and TG in function of the stoppage hydration technique, J. Therm. Anal. Calorim. 136 (2019) 1269–1284, https://doi.org/10.1007/s10973-018-7734-5.
[53] J.J. Thomas, H.M. Jennings, J.J. Chen, Influence of nucleation seeding on the hydration mechanisms of tricalcium silicate and cement, J. Phys. Chem. C 113 (2009) 4327–4334, https://doi.org/10.1021/jp809811w.
[54] S. Rahimi-Aghdam, Z.P. Bažant, M.J. Abdolhosseini Qomi, Cement hydration from hours to centuries controlled by diffusion through barrier shells of C-S-H, J. Mech. Phys. Solid. 99 (2017) 211–224, https://doi.org/10.1016/j.jmps.2016.10.010.
[55] S. Bishnoi, K.L. Scrivener, Studying nucleation and growth kinetics of alite hydration using μic, Cement Concr. Res. 39 (2009) 849–860, https://doi.org/10.1016/j.cemconres.2009.07.004.
[56] R. Alizadeh, L. Raki, J.M. Makar, J.J. Beaudoin, I. Moudrakovski, Hydration of tricalcium silicate in the presence of synthetic calcium–silicate–hydrate, J. Mater. Chem. 19 (2009) 7937–7946, https://doi.org/10.1039/B910216G.
[57] H. Justnes, E.C. Nygaard, Technical calcium nitrate as set accelerator for cement at low temperatures, Cement Concr. Res. 25 (1995) 1766–1774, https://doi.org/10.1016/0008-8846(95)00172-7.
[58] H. El-Didamony, A.M. Sharara, I.M. Helmy, S.A. El-Aleem, Hydration characteristics of β-C2S in the presence of some accelerators, Cement Concr. Res. 26 (1996) 1179–1187, https://doi.org/10.1016/0008-8846(96)00103-2.
[59] A. Kičaitė, I. Pundienė, G. Skripkiūnas, The influence of calcium nitrate on setting and hardening rate of Portland cement concrete at different temperatures, IOP Conf. Ser. Mater. Sci. Eng. 251 (2017), 012017, https://doi.org/10.1088/1757-899X/251/1/012017.
[60] H. Choi, M. Inoue, H. Choi, J. Kim, Y. Sudoh, S. Kwon, B. Lee, A. Yoneyama, Physicochemical study on the strength development characteristics of cold weather concrete using a nitrite–nitrate based accelerator, Materials 12 (2019) 2706, https://doi.org/10.3390/ma12172706.
[61] Q. Li, Y. Wang, G. Geng, H. Chen, P. Hou, X. Cheng, P.J. Monteiro, S. Huang, J. H. Kim, Microstructural study of hydration of C3S in the presence of calcium nitrate using scanning transmission X-ray microscopy (STXM), J. Nanomater. 2020 (2020).
[62] J.Q. Dumm, P.W. Brown, Phase assemblages in the system Ca(OH) $_2$ —Al $_2$ O $_3$ —Ca(NO $_3$) $_2$ —H $_2$ O, Adv. Cement Res. 8 (1996) 143–153, https://doi.org/10.1680/adcr.1996.8.32.143.
[63] E.B. Ogunbode, I.O. Hassan, Effect of Addition of Calcium Nitrate on Selected Properties of Concrete Containing Volcanic Ash, 2011, p. 10.
[64] N. Chikh, M. Cheikh-Zouaoui, S. Aggoun, R. Duval, Effects of calcium nitrate and triisopropanolamine on the setting and strength evolution of Portland cement pastes, Mater. Struct. 41 (2008) 31–36, https://doi.org/10.1617/s11527-006-9215-8.
[65] L. Xu, K. Wu, N. Li, X. Zhou, P. Wang, Utilization of flue gas desulfurization gypsum for producing calcium sulfoaluminate cement, J. Clean. Prod. 161 (2017) 803–811, https://doi.org/10.1016/j.jclepro.2017.05.055.
[66] F.-M. Raoult, Loi générale des tensions de vapeur des dissolvants, C. R. Hebd. Seances Acad. Sci. 104 (1887) 1430–1433.
[67] É. Clapeyron, Mémoire sur la puissance motrice de la chaleur, J. LÉcole Polytech. 14 (1834) 153–190.
[68] M. Chai, J. Zhang, H. Zhang, Y. Mu, G. Sun, Z. Yin, A method for calculating unfrozen water content of silty clay with consideration of freezing point, Appl. Clay Sci. 161 (2018) 474–481, https://doi.org/10.1016/j.clay.2018.05.015.
[69] B.R. Puri, L.R. Sharma, M.L. Lakhanpal, Freezing point of water held in porous bodies at different vapor pressures, J. Phys. Chem. 58 (1954) 289–292, https://doi.org/10.1021/j150514a001.
[70] P. Pipilikaki, M. Beazi-Katsioti, The assessment of porosity and pore size distribution of limestone Portland cement pastes, Construct. Build. Mater. 23 (2009) 1966–1970, https://doi.org/10.1016/j.conbuildmat.2008.08.028.
[71] L.G. Homshaw, High resolution heat flow DSC: application to study of phase transitions, and pore size distribution in saturated porous materials, J. Therm. Anal. Calorim. 19 (2005) 215–234, https://doi.org/10.1007/bf01915798.
[72] A. Yoneyama, H. Choi, M. Inoue, J. Kim, M. Lim, Y. Sudoh, Effect of a nitrite/nitrate-based accelerator on the strength development and hydrate formation in cold-weather cementitious materials, Materials 14 (2021) 1006, https://doi.org/10.3390/ma14041006.
[73] M. Balonis, M. Mędala, F.P. Glasser, Influence of calcium nitrate and nitrite on the constitution of AFm and AFt cement hydrates, Adv. Cement Res. 23 (2011) 129–143, https://doi.org/10.1680/adcr.10.00002.
[74] W. Franke, M. Balonis, T. Oey, G. Sant, THE FATE OF NITRATE IONS IN CONCRETE UNDER THE FOCUS OF CORROSION INHIBITION, 2014.
[75] A. Duran, R. Sirera, M. Pérez-Nicolás, I. Navarro-Blasco, J.M. Fernández, J. I. Alvarez, Study of the early hydration of calcium aluminates in the presence of different metallic salts, Cement Concr. Res. 81 (2016) 1–15, https://doi.org/10.1016/j.cemconres.2015.11.013.
[76] L. Huang, Z. Yang, Hydration kinetics of tricalcium silicate with the presence of portlandite and calcium silicate hydrate, Thermochim. Acta 681 (2019) 178398, https://doi.org/10.1016/j.tca.2019.178398.
[77] M. Shan-bin, Z. Zhao-jia, The early strength of slag cements with addition of hydrate microcrystals, J. Wuhan Univ. Technol.-Materials Sci. Ed. 17 (2002) 83–85, https://doi.org/10.1007/BF02832630.
[78] D. Wang, X. Yao, T. Yang, W. Xiang, Y. Feng, Y. Chen, Controlling the early-age hydration heat release of cement paste for deep-water oil well cementing: a new composite designing approach, Construct. Build. Mater. 285 (2021) 122949, https://doi.org/10.1016/j.conbuildmat.2021.122949.
[79] L. Liu, G. Ye, E. Schlangen, H. Chen, Z. Qian, W. Sun, K. van Breugel, Modeling of the internal damage of saturated cement paste due to ice crystallization pressure during freezing, Cement Concr. Compos. 33 (2011) 562–571, https://doi.org/10.1016/j.cemconcomp.2011.03.001.
[80] D.P. Bentz, Low Temperature Calorimetry Studies of Hydrating Portland Cement Pastes, National Institute of Standards and Technology, Gaithersburg, MD, 2005, https://doi.org/10.6028/NIST.IR.7267.
[81] E. Kamada, Frost damage of concrete considering freezing point depression of capillary water in hardened cement paste. https://eprints.lib.hokudai.ac.jp/dspace/bitstream/2115/42180/1/145_53-62.pdf, 1988.
[82] E.N. Ashworth, F.B. Abeles, Freezing behavior of water in small pores and the possible role in the freezing of plant tissues, Plant Physiol 76 (1984) 201–204.
[83] T.C. Powers, Freezing effects in concrete, Spec. Publ. 47 (1975) 1–12, https://doi.org/10.14359/17603.
[84] G. Fagerlund, Determination of pore-size distribution from freezing-point depression, Mater. Construcción 6 (1973) 215–225, https://doi.org/10.1007/BF02479036.
[85] H. Huang, X. Shen, Statistical study of cement additives with and without chloride on performance modification of Portland cement, Prog. Nat. Sci. Mater. Int. 21 (2011) 246–253, https://doi.org/10.1016/S1002-0071(12)60038-0.
[86] M.P. Kumar, K.M. Mini, M. Rangarajan, Ultrafine GGBS and calcium nitrate as concrete admixtures for improved mechanical properties and corrosion resistance, Construct. Build. Mater. 182 (2018) 249–257, https://doi.org/10.1016/j.conbuildmat.2018.06.096.
[87] S. Motoki, M. Inoue, H. Choi, S. Sekita, S. Fukuchi, Control of Curing Temperature of Cold-Weather Concrete through Effective Utilization of Energy-Saving Heat-Curing Systems, (n.d.) 8.
[88] R. Fitzgerald, S. Sithole, Preliminary experiences with a falling-film evaporator pilot plant, 1991, p. 5.